Design and Validation of High Speed Active Trailer Steering System for Articulated Heavy Vehicle

by

Zhituo Ni

Thesis submitted to the

University of Ontario Institute of Technology

in the fulfillment of the

Requirement for the degree of

Master of Engineering

in

Mechanical Engineering

Oshawa, Ontario, Canada, 2016

Abstract

Articulated heavy duty vehicles are widely used around the world for its economic and environmental benefits. A-train double is one of the most popular heavy duty vehicles in Canada. Despite its advantages, the spread of A-train is hampered by poor lateral dynamic performance and poor accident avoid ability in highway resulted from its special structure. In order to evaluate the lateral dynamic performance of the A-train double at highway speed, ISO standards have proposed the rearward amplification (RA) measures to characterizing the performance. It has been reported that the RA curves obtained through three different methods proposed by ISO-14791 differ. This thesis studies three proposed methods in detail and analyzes the contributing causes for the inconsistency among three test maneuvers based on A-train double. In order to increase the lateral stability of the A-train double, Active steering systems (ATS) have been designed through two methods: robust LQR-LMI method with genetic algorithm (GA) optimization and H_∞ method. The designed controllers are validated by numerical simulation and hardware in-loop simulation. The ATS designed from two methods show good robust stability and improve the lateral dynamic performance of A-train double dramatically at highway speed.

Acknowledgement

I am grateful to my supervisor Dr. Yuping He for his support, guidance during this research. Thank him to give me this chance to work on vehicle dynamics and modeling. Without him, it is impossible for me to get insight of automotive dynamics and finish this paper.

I would also like to thank the members of my research group who gave me some advice during this research. Last but not least, I appreciate my family and all my good friends at UOIT, whose friendship and support throughout this research was invaluable.

Table of Contents

List of Figures

List of Tables

Nomenclature

a	Longitudinal distance between front axle and the center of gravity of the tractor
AFRM	Automated frequency response method
AHV	Articulated heavy vehicle
b	Longitudinal distance between the center of gravity and the first rear axle of the tractor
C_d	Cornering stiffness of the axle of the dolly of A-Train
C_f	Cornering stiffness of the front axle of the tractor of A-Train
C_r	Cornering stiffness of the rear axle of the tractor of A-Train
C_{t1}	Cornering stiffness of the axle of the first semitrailer of A-Train
C_{t2}	Cornering stiffness of the axle of the second trailer of A-Train
CG	Center of gravity
d	Longitudinal distance between the center of gravity of the tractor and the first hitch point
DOF	Degree of freedom
DTAHV	Double trailer articulated heavy vehicle
e	Longitudinal distance between the center of gravity of the first semitrailer and the first hitch point

e'	Longitudinal distance between the center of gravity of the dolly and the second hitch point
$f_1(\alpha_1)$	Lateral force on the first axle of double trailer articulated heavy vehicle
$f_2(\alpha_2)$	Lateral force on the second axle of double trailer articulated heavy vehicle
$f_3(\alpha_3)$	Lateral force on the third axle of double trailer articulated heavy vehicle
$f_4(\alpha_4)$	Lateral force on the fourth axle of double trailer articulated heavy vehicle
$f_5(\alpha_5)$	Lateral force on the fifth axle of double trailer articulated heavy vehicle
g	Acceleration of gravity
h	Longitudinal distance between the center of gravity of the first semitrailer and the first semitrailer's axle
h'	Longitudinal distance between the center of gravity of the dolly and the dolly's axle
h_1	Height of the center of gravity of the sprung mass of the second semitrailer of the B-Train, measured from the roll center
h_2	Height of the roll center, measured from the center of gravity of the unsprung mass of the second semitrailer of the B-Train
h_3	Height of the center of gravity of the unsprung mass of the second semitrailer of the B-Train, measured from ground
I_1	Yaw moment of inertia of the tractor
I_d	Yaw moment of inertia of the dolly

I_{t1}	Yaw moment of inertia of the first semitrailer
I_{t2}	Yaw moment of inertia of the second trailer
j	Longitudinal distance between the center of gravity of the first semitrailer and the second hitch point
j'	Longitudinal distance between the center of gravity of the dolly and the third hitch point
k	Longitudinal distance between the center of gravity of the second trailer and the third hitch point
l	Longitudinal distance between the center of gravity of the second trailer and the second trailer's axle
LCV	Long combination vehicles
m_1	Total mass of the tractor
m_d	Total mass of the dolly
m_s	Sprung mass of the second semitrailer of the B-Train
m_{t1}	Total mass of the first semitrailer
m_{t2}	Total mass of the second trailer
MCSSI	Multiple cycle sine-wave steering input
PID	Proportional–integral–derivative
r_1	Yaw rate of the tractor

r_2	Yaw rate of the first semitrailer
r_3	Yaw rate of the third unit of double trailer articulated heavy vehicle
r_4	Yaw rate of the fourth unit of double trailer articulated heavy vehicle
RA	Rear amplification
TTB	Trajectory tolerance band
U	Forward speed of the vehicle
V_1	Lateral speed of the tractor
V_2	Lateral speed of the first semitrailer
V_3	Lateral speed of the third unit of double trailer articulated heavy vehicle
V_4	Lateral speed of the fourth unit of double trailer articulated heavy vehicle
α	Side-slip angle of the axle
α_1	Side-slip angle of the first axle of double trailer articulated heavy vehicle
α_2	Side-slip angle of the second axle of double trailer articulated heavy vehicle
α_3	Side-slip angle of the third axle of double trailer articulated heavy vehicle
α_4	Side-slip angle of the fourth axle of double trailer articulated heavy vehicle
α_5	Side-slip angle of the fifth axle of double trailer articulated heavy vehicle
δ	Steering angle of the front axle of the tractor

Chapter 1

Introduction

1.1 Long Combination Vehicle Background

Ontario Long combination vehicles (LCV) consist of specially equipped tractors pulling two full-sized semi-trailers. They may operate on specified 400-series highways between Quebec and Ontario. LCVs were introduced into Ontario in 2009 as a public-private partnership between the Ontario Ministry of Transportation (MTO) and the Ontario Trucking Association (OTA). LCVs are good for manufacturers, consumers and environment. Ontario is now allowing up to 1,600 LCVs on designated highways. In 2014, participating carriers completed over 36,000 one-way LCV trips, over 11 million kilometres of travel. When comparing an LCV to the two tractor trailers they replace, LCVs have eliminated 11 Million tonnes of greenhouse gas emissions from entering our environment. By using less fuel to carry goods, LCVs reduce the greenhouse gas emissions (GHGs) associated with shipping goods by approximately one-third. In addition, allowing LCVs will enable shippers to move goods more efficiently between Ontario and Quebec, since Quebec has allowed these trucks on their roads for more than 20 years. They allow Ontario retailers and manufacturers to bring light-weight, bulky goods to market at a lower cost. [1].

The LCV researched in this thesis is A-train double, which are the most commonly used across Canada for goods transportation. As is shown in Fig1.1, the LCV A-train double consists of a tractor and two semi-trailers connected by a converter dolly. The tractor provides power for the vehicle combination, and the driver can control front steering axle by turning the steering wheel. The dimensions, weight requirements and restrictions of the A-Train double is described at length in [2].

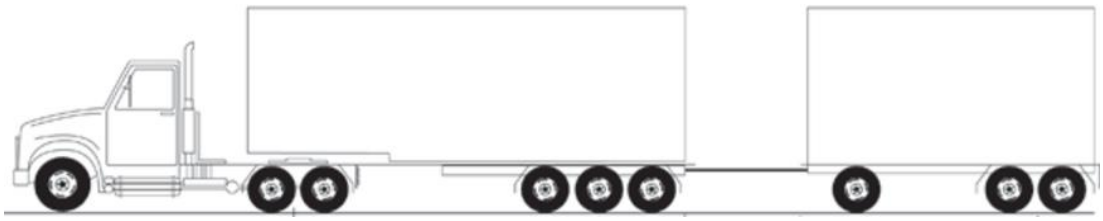

Figure 1.1. Configuration of mechanical couplings of A-Train double

1.2 Motivations and Objectives

A review of heavy vehicle accidents in the U.S and Canada revealed that heavy trucks were involved in 28% of single vehicle accidents, as compared with 19% for passenger vehicles [3]. Almost 23% of the heavy vehicle accidents were either associated with or resulted in rollover [4]. Highway accidents involving heavy vehicles cause greater damage and injury than other accidents. In the U.S., there are over 15,000 rollovers of commercial trucks each year among which about 9,400 are rollovers of tractor-semitrailers. Around 58% of the fatal injuries to the truck driver occurred in rollover crashes [5].

The low level roll stability of LCV sets them apart from light vehicles and appears to be a contributing cause of rollover accidents. The basic measure of roll stability is the static rollover threshold expressed as lateral acceleration in gravitational units (g). Most passenger cars have rollover thresholds around 1 g ranging from 0.8 to 1.2 g. However, the rollover threshold of a loaded LCV often lies below 0.5 g. A number of standards have been established or proposed for the roll threshold of heavy vehicles. New Zealand has a minimum roll threshold of 0.35 g for all heavy vehicles [6]. If the lateral acceleration exceeds the static rollover limit, it need only be sustained for a finite time to result in rollover. For example, for a typical heavy truck, acceleration of 110 percent of the static limit can produce rollover if sustained for about 1 second; 120 percent need be sustained for only about 0.6 seconds [5].

Directional dynamics of LCVs are investigated to derive their handling, directional control and directional stability characteristics under transient and steady steering maneuvers. The steady-state handling performance of a vehicle is concerned with its directional behavior during a turn under time invarying conditions. A unified measure of steady-state handling performance was proposed, i.e., the low-speed 90 degree intersection turn. The steady-stare directional dynamic response determines the vehicle handling and rollover limit under steady turning maneuvers, whereas the transient directional dynamic response is concerned with roll and yaw instabilities under transient maneuvers. Both static and dynamic stability

of heavy articulated vehicles are important issues to be considered when evaluating the behavior of LCVs.

In view of the growing highway safety concern related to dynamic performance of LCVs, many scholars have concentrated on the safety performance of LCVs. The vehicle stability and control performance at highway speed is described through two essential performance attributes relevant to safety: rearward amplification, transient high-speed off-track distance.

For A-train double that will be studied in the thesis, it was concluded that the lateral constraint force at the pintle hitch of a typical A-train double is relatively small and that the directional response of vehicles can involve large amounts of rearward amplification (RA). Therefore, although the application of A-train can bring about economic and environmental benefits, however, the A-train double configuration is considered undesirable because of its low stability at highway speeds due to their complex structure, heavy payload and high center of gravity.

It is relatively hard for truck drivers to perceive their proximity to rollover while driving. Since the LCV driver sits in the tractor and adjusts the steering wheel angle responding to the performance of the tractor, the following trailers tend to oscillate and exaggerate the lateral movement of the tractor. In this case, even the tractor is well driven by the driver, however, the trailers may reach the rollover threshold limit.

The evaluation of LCV lateral dynamic performance has been the focus of the various research efforts for more than half a century. Evaluating the lateral dynamic performance is no easy task since the complicated interactions among the driver/vehicle/trailer/road. The lateral stability of the LCV is a most important part of active vehicle safety and traffic safety [7, 8]. RA which describes the tendency of the trailer to exaggerate the lateral motion of the preceding tractor during some kind of the maneuvers is brought forward to characterizing lateral stability. The International Organization for Standardization released the test maneuvers for determining RA measure in ISO-14791. In ISO-14791, RA is mathematically define as a ratio of the lateral acceleration of the rearmost trailer to that of the tractor. ISO-14791 recommends two time domain methods and one frequency domain method to derive RA through experiments. The RA measure is an important indicator for vehicle maneuverability and accident avoid ability since LCV with lower level of RA characteristics face less risk of rollover during obstacle avoidance maneuvers (Fancher and Winkler, 1992, J. Woodrooffe and P. Milliken, 2007) [9-10]. The large level distortion of the lateral acceleration of the tractor may lead to rollover or a swing-out of the rearmost trailer.

It has been reported that the RA obtained from three different methods proposed by ISO-14791 differs in some degree [11]. This thesis studies the proposed RA test maneuvers in

details and analyzes the contributing causes for the inconsistency among different test maneuvers based on A-train double.

To increase the maneuverability and lateral performance of the LCVs, many scholars have already devised many different kinds of active safety systems to achieve the desired lateral dynamic response [12, 13]. In view of A-train double, because of its low stability at highway speeds, the purpose of the active safety system is to reduce the RA measure in concerned frequency range and reduce the maximum transient off-track distance according to ISO-14791.

With lower RA ratio under the concerned frequency, the magnitude of the trailer's lateral acceleration is kept away from the unstable region. For example, the RA measure for A-train double around 0.4 Hz steering input is around 2 and the rollover threshold limit for A-train double is around 0.35 g [14]. In this case, the maximum acceleration of the tractor cannot exceed 0.175 g which constrains the lateral performance and maneuverability for the A-train double. With low limit of the lateral acceleration, the accident avoid ability is also hampered in some degree.

As the active safety system can reduce the RA measures and maximum transient off-track distance, the LCVs will have more obstacle avoidance ability and less opportunity to rollover. A lot of control algorithms [15-18] can be applied to designing the active safety

system such as linear quadratic regulator (LQR) algorithm, sliding mode algorithm and H_∞ algorithm.

However, unlike other current systematic control design procedures like H_∞ or sliding mode control, classic LQR controller cannot cope with system parameter uncertainty. This thesis proposes the robust LQR-LMI algorithm with genetic algorithm (GA) method to deal with the parameter uncertainty problem in designing the ATS for A-train double in highway. Furthermore, the ATS for A-train at highway speeds is also designed through H_∞ control method. The controllers designed from two methods are then validated through numerical simulation and hardware in-loop system simulation. The RA curves and maximum off-track distance of A-train double with ATS controllers are obtained to evaluate the lateral dynamic performance of the system at highway speeds.

All in all, the objectives of this thesis can be summarized as:

1) Compare and contrast three test maneuvers determining the RA measure proposed in ISO-14791 based on A-train double;

2) Design the ATS for A-train at highway speeds through robust LQR-LMI with GA optimization method and validate the designed controller in numerical simulation and hardware in-loop system simulation;

3) Design the ATS for A-train double at highway speeds through H_∞ robust control method and validate the designed ATS control in numerical simulation. The designed high speed ATS controller is evaluated through two essential performance attributes: rearward amplification, transient high-speed off-track proposed in ISO-14791.

1.3 Thesis Organization

The thesis is organized as follow. Chapter 1 provides the background information of LCV system, and introduces the motivations and objectives of this research. Chapter 2 offers a literature review on the RA test maneuvers and the previous ATS design approaches. Chapter 3 describes the derivation of the 5 DOF yaw-plane model for A-train double and validates the model with TruckSim software. Chapter 4 discusses the inconsistency problem of the three testing methods proposed by ISO 14791. Chapter 5 proposes the ATS controller for high speed A-train double designed from robust LQR-LMI method with GA optimization and then validates the controller through numerical simulation and hardware in-loop simulation. The designed high speed ATS controller is evaluated through two essential performance attributes: rearward amplification, transient high-speed off-track proposed in ISO-14791. Chapter 5 shows the design of ATS controller of A-train double at high speed through H_∞ method. Then the designed controller is validated through numerical simulation. Finally, the summary and the conclusions of the research are provided in Chapter 7.

Chapter 2

Literature Review

2.1 Introduction

This chapter presents a comprehensive literature review on the research related to RA test maneuvers proposed in ISO-14971 and introduces the inconsistency problem in previous literature. RA is a parameter to describe the lateral stability for LCVs. Based on previous literature, it has been found that the RA results tested from different test maneuvers differ in some degree. To increase the lateral stability of LCVs, ATS is introduced to improve the maneuverability and safety of the A-train in highway. Various control methods applied to the ATS designing are illustrated in details based on previous literature. These control methods all show good simulation results to increase the lateral stability and safety of the LCVs.

2.2 Literature Review on Test Maneuvers

As is illustrated in chapter 1, RA which describes the tendency of the trailer to exaggerate the lateral motion of the preceding tractor is brought forward to characterizing lateral dynamic performance for LCVs. In ISO-14791, RA is mathematically defined as a ratio of the lateral acceleration of the rearmost trailer to that of the tractor. The LCVs with small

RA measures under concerned frequency is likely to face less risk of rollover during obstacle avoidance maneuvers.

In 1992, Fancher and Winkler put forward a test methodology named “single lane change” to quantify RA [9]. The test driver follows the prescribed trajectory under the test maneuver. This method deals successfully with the nonlinearities of vehicle system and produces a reliable measure of rearward amplification. However, the test can produces substantially different results depending on how the path is chosen within the tolerance band [14].

In 2000, the International Organization for standardization released the standard test procedures in ISO-14791. Three different test procedures for determining RA of LCVs are described in details [19]: 1) an open-loop test procedure with a single sine wave steering input 2) a driver closed-loop trajectory following method based on accident avoid maneuver. 3) random steering input based on frequency domain procedure. For open-loop test procedure, one full period sinusoidal steering input is applied to the steering wheel, followed by a period of neutral steering-wheel position. The gain of the lateral acceleration is measured in the time domain. The justification for this test maneuver is that this form of lateral acceleration will result in an obstacle avoidance maneuver in which the vehicle translates sideways [9]. For closed-loop test procedure, an experienced driver in closed-loop performed as a regulator to push the LCVs follow a predefined path. The main reason for deciding to develop a prescribed path approach has been to provide a common basis for

different LCVs. This has not always been possible using a specified input at the steering wheel because different tractors performed different maneuvers even with identical steering angle input. For random steering input frequency domain procedure, the random steer input is applied to the steering system by a driving machine. This method produces a complete system gain in the frequency domain. The limit of the input is determined for a lateral acceleration level within the range in which the vehicle exhibits linear behavior.

The experiment test results from the three methods, however, differ in some degree [7]. Some scholar have already done some work for this topic. In 1995, J.Preston. Thomas and M.El. Gindy reported that the path tolerance has some influence on the experiment error when determining the RA [11]. In 2016, Wang, Qiushi, and He, Yuping reported that the transient response of the tractor lateral acceleration occurred under the open-loop test maneuver impose a non-neglected impact on the RA measures of LCVs [20].

In order to study the inconsistency problem of the three testing methods proposed by ISO-14791, the model for the LCV with a A-train double configuration is developed using Trucksim software based on the prescribed dimension and weight limits offered in [21]. Another frequency domain method named automated frequency response measuring technique (AFRM) proposed in [22] is also applied in this paper to validate accuracy of the RA value.

2.3 Literature Review on ATS Design Approach

ATS is able to operate in two modes: low speed mode and high speed mode. For low speed mode, ATS is activated to improve the low speed path following ability of the A-train double. The control objectives of ATS for A-train double at highway speeds are: 1) reduce the A-train's RA measures in the concerned frequency range at high speed with small control effort to satisfy desirable transient characteristics, 2) reduce high speed maximum transient off-track distance, 3) robust stability requirement for the control system with time varying parameters and enough robust performance to reject certain disturbances. The first objective is to increase lateral stability of the rearmost trailer and to maintain the peak lateral acceleration of the rearmost trailer within the rollover limit. Ideally, the RA should be kept around 1 during the interested frequency domain. In this way, the rearmost trailer wouldn't rollover when the tractor performs well. The drivers could have a better control over the LCVs. The safety of the LCVs is improved. The second requirement for the maximum off-track distance is to increase the maneuverability and accident avoid ability during the lane change. The third target is the requirement of a controller since there are many factors influencing a real-world vehicle running on the highway such as forward speed, road condition, weather and so on. The performance of a well-designed controller should be assured even under the worst condition.

The LQR is a well-known design technique that provide practical feedback gains. The classic LQR approach deals with optimization of a cost function or performance index. Thus, the designer can weight which states and which inputs are more important in the control action to seek for appropriate transient and steady-state performances [23]. Specifically, in the field of vehicle dynamics, the choice of the cost function parameters is advantageous, since it can be used to minimize the RA and roll angle. It is also worth to point out that the closed-loop system with such LQR controller presents interesting properties like a 60 degree phase margin and an infinite gain margin [24]. In 2008, C. Cheng and D. Cebontake take advantage of LQR control algorithm to improve the roll stability of tractor semi-trailer using active semi-trailer steering [25]. In 2010, Yuping He presents an integral design method for active steering system of B-train double to increase the path following ability and lateral stability. [26]. However, unlike other current systematic control design procedures like H_∞ or sliding mode, classic LQR control cannot cope with system uncertainty.

H_∞ Control method is a frequency domain method for robust control. The ATS controller designed through the H_∞ method will satisfy not only the robust stability requirements but minimize the H_∞ norm from the disturbances to weighted performances as well. In 2000, Jeng-Yu Wang and Masayoshi Tomizuka proposed a robust steering controller using H_∞ loop shaping procedure for a tractor semitrailer combination to increase trajectory

following ability in low speed below 40km/h [27]. In 2004, Rongrong Wang, Hui Zhang and Junmin Wang present a linear parameter-varying control strategy to preserve stability and improve the handling of four-wheel ground vehicle [16]. An LQR-based H_∞ controller is devised to tradeoff between the tracking performance and the control input energy. In 2016, Zhilin Zhang, Lei Zhang and etc present hydraulic brake system optimized by H_∞-GA method to improve the anti-roll performance of the vehicle [28].

GA is widely used in optimization of the ATS controllers. In most case, however, GA is nothing else than probabilistic optimization method which are based on the principle of evolution. This idea is first brought out by J. D. Bagley in [29]. The theory and applicability was then strongly influenced by J. H. Holland, who can be considered as the pioneer of genetic algorithm [30].The transition from one generation to the next consists of four basic components: selection, crossover, mutation, and sampling. Selection is the mechanism for selecting individuals for reproduction according to their fitness (objective function value). Crossover is the procedure of merging the genetic information of two individuals. If coding is chosen properly, two good parents will produce good children. Mutation can be realized as a random deformation of the strings with a certain probability. Through sampling, the new generation is created from previous one and its offspring [31].

Artificial intelligent (AI) assumes that human intelligence can be so precisely described that a machine can be made to simulate it [32]. In this way, the machines can obtain the

human intelligence to solve certain problems by learning from the behavior of a human. Furthermore, the intelligent control are able to be applied to studying real problems in the world. Many AI technologies such as artificial neural network control and fuzzy logic control algorithms have been demonstrated and are routinely used with enormous success in many domain especially in vehicle application.

Fuzzy logic control theory is based on linguistic synthetics and doesn't need an exact model to design the control systems. The designed fuzzy logic controller possesses more robust compared with other controller. In [33], a hybrid fuzzy logic approach has been proposed to improve the ride comfort of passengers. Compared with PID controller, the designed controller is able to reduce vibration of the nonlinear half-vehicle model. Niels J. Schouten in [34] had developed a fuzzy logic controller for hybrid vehicles to optimize the operational efficiency of component. The results show that the overall improvement of the fuzzy logic controller for an urban cycle equals 6.8%. Yi-Jen Mon and Chih-Min Lin in [35] had developed a supervisory recurrent fuzzy neural network control to deal with the vehicle collision avoidance system, which is an uncertain nonlinear model-free system. The simulation results show that the performance and effectiveness of the controller is better than that obtained from formal formula-based controllers.

This thesis proposes LQR-LMI method with GA optimization to tackle the parameter uncertainty problem in LQR method. In practice, the ATS parameters such as the time

delay caused by the ATS actuator and forward speed of the train are considered as parameter variables since these variables greatly influence the performance of the A-train double. The ATS for A-train double at highway speeds is also designed through H_∞ method. Both of the controllers are validated by numerical simulation and hardware in-loop simulation. What's more, the performance of closed-loop system is evaluated by the RA curve and maximum off-track distance illustrated in ISO standards.

Chapter 3

Modeling and Validation for A-train double

3.1 Introduction

A real vehicle is a highly nonlinear system due to the nonlinear tires, vehicle air dynamic, asymmetric steering system and kingpin effects. In order to research some certain characteristics of the vehicle dynamics, many nonsignificant effects are simplified or neglected and only the main dynamic effects are remained deliberately. In this way, the highly nonlinear vehicle are even considered as a mechanical rigid body in some situation depending on the interested part of the researcher. In this chapter, a 5 DOF yaw-plane mathematic model of the A-train double is deduced through the rigid body dynamics to analysis lateral dynamic performance of the vehicle. The accuracy and fidelity of these linear models are validated with commercial software TruckSim. This mathematic model of A-train double lays the foundation for designing the ATS controller which will be illustrated in the following chapters.

3.2 Derivation of Yaw-Plane Models

For linear yaw-plane model derivation, A-train double is considered under operations on a 2-demision road. Based on the body-fixed coordinate systems and Newton's second law,

the equations of motion can be generated.

3.2.1 Assumptions

In order to obtain the mathematic model containing the main dynamic performance of the train, reasonable assumptions are made to simplify vehicle models. For vehicle modelling in this research, the assumptions are made as follows:

(1) each vehicle unit is considered as a rigid body;

(2) each axle is represented by a single wheel;

(3) the vehicle's forward speed U and the steering angle δ of tractor's front axle are given;

(4) the vertical movement, pitch and roll motions, the braking and the aerodynamic forces are neglected;

(5) the relation between the lateral force of a tire and the side-slip angle is determined by a linear function; and

(6) the articulated angles between two adjacent units are small.

3.2.2 Derivation of 5 DOF Yaw-Plane Model for A-Trains

For the simplified A-train double model shown in Figure 1, the motion considered in this model are (V_1, r_1), (V_2, r_2), (V_3, r_3) and (V_4, r_4), which are lateral velocity and yaw rate for the tractor, the first trailer, dolly and the second trailer respectively. From Newton's second law, the governing equations of motion can be generated.

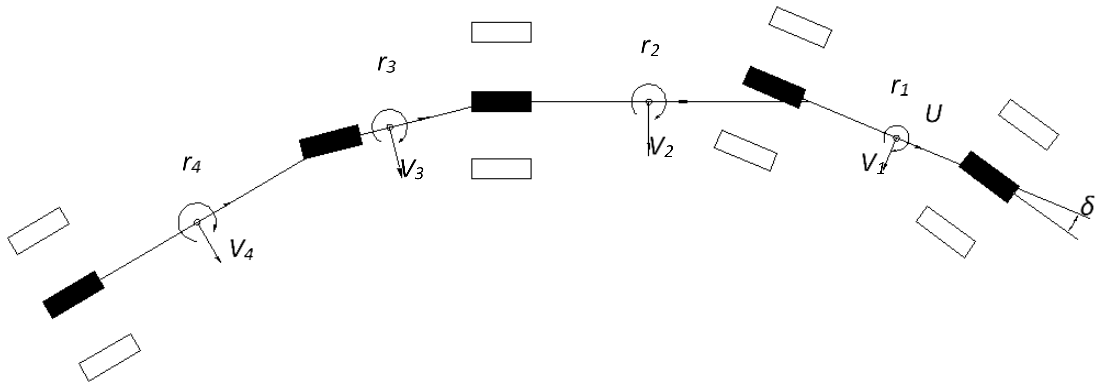

Figure 3.1. Top view of the 5DOF yaw-plane model for A-Trains

The equations of motion for the tractor are

$$m_1(\dot{V}_1 + Ur_1) = f_1(\alpha_1) + f_2(\alpha_2) - Y_1 \tag{3.1}$$

$$I_1\dot{r}_1 = af_1(\alpha_1) - bf_2(\alpha_2) + dY_1 \tag{3.2}$$

The equations of motion for the first trailer are

$$m_{t1}(\dot{V}_2 + Ur_2) = f_3(\alpha_3) + Y_1 - Y_2 \tag{3.3}$$

$$I_{t1}\dot{r}_2 = eY_1 - hf_3(\alpha_3) + jY_2 \tag{3.4}$$

The equations of motion for the dolly are

$$m_d(\dot{V}_3 + Ur_3) = f_4(\alpha_4) + Y_2 - Y_3 \tag{3.5}$$

$$I_d\dot{r}_3 = e'Y_2 - h' f_4(\alpha_4) + j'Y_3 \tag{3.6}$$

And the equations of motion for the second trailer are

$$m_{t2}(\dot{V}_4 + Ur_4) = f_5(\alpha_5) + Y_3 \tag{3.7}$$

$$I_{t2}\dot{r}_4 = kY_3 - lf_5(\alpha_5) \tag{3.8}$$

The side-slip angles of the axles are

$$\alpha_1 = \frac{V_1 + ar_1}{U} - \delta \tag{3.9}$$

$$\alpha_2 = \frac{V_1 - br_1}{U} - \delta_2 \tag{3.10}$$

$$\alpha_3 = \frac{V_2 - hr_2}{U} - \delta_3 \tag{3.11}$$

$$\alpha_4 = \frac{V_3 - h'r_3}{U} - \delta_4 \tag{3.12}$$

$$\alpha_5 = \frac{V_4 - lr_4}{U} - \delta_5 \tag{3.13}$$

Adjacent vehicle units are connected at the 'fifth wheel' or hitch, hence velocities at the hitch point using either set of axes must be compatible. The equation of velocity at first hitch point is shown as below, in which, *U* is the forward speed of the vehicle.

$$V_2 + er_2 = V_1 - dr_1 + U(\psi_1 - \psi_2) \tag{3.14}$$

The equation of velocity at second hitch point is

$$V_3 + e'r_3 = V_2 - jr_2 + U(\psi_2 - \psi_3) \tag{3.15}$$

The equation of velocity at third hitch point is

$$V_4 + kr_4 = V_3 - j'r_3 + U(\psi_3 - \psi_4) \tag{3.16}$$

Equations (3.14), (3.15) and (3.16) can be rewritten as

$$\dot{V}_2 + e\dot{r}_2 = \dot{V}_1 - d\dot{r}_1 + Ur_1 - Ur_2 \tag{3.17}$$

$$\dot{V}_3 + e'\dot{r}_3 = \dot{V}_2 - j\dot{r}_2 + Ur_2 - Ur_3 \tag{3.18}$$

$$\dot{V}_4 + k\dot{r}_4 = \dot{V}_3 - j'\dot{r}_3 + Ur_3 - Ur_4 \tag{3.19}$$

The notation for the above equations is provided in Appendix 2. By eliminating the reaction forces at the hitch point, i.e. Y_1, Y_2, Y_3, and using the linear tire model to represent the lateral tire force, we can write the equations of motion of 5 DOF yaw-plane model into the state space form, in which u is the control input of the third axle and δ is the steering angle input of the driver.

$$\dot{x} = \mathbf{A}x + \mathbf{B_u}u + \mathbf{B_d}\delta \tag{3.20}$$

In Equation (3.20), the state variable vector x is defined as

$$x = [V_1 \quad r_1 \quad V_2 \quad r_2 \quad V_3 \quad r_3 \quad V_4 \quad r_4]^T \tag{3.21}$$

In Equation (3.20), **A**, $\mathbf{B_u}$ and $\mathbf{B_d}$ are the system matrix, the input matrix and disturbance matrix respectively.

3.3 Validation of the 5 DOF Yaw-plane Model for A-Trains

3.3.1 TruckSim Model for A-Trains

TruckSim delivers the most accurate, detailed, and efficient methods for simulating the performance of multi-axle commercial and military vehicles. With more than twenty years of real-world validation, TruckSim is universally the preferred tool for analyzing vehicle

dynamics. TruckSim are used worldwide by over 110 OEMs and Tier 1 suppliers and over 200 universities and government research labs [36]. The configuration of the TruckSim model for A-train double is illustrated as “S_S+S+dS+S”, where the character ‘S’ represents a solid axle, the character ‘d’ represents a dolly, the underline indicates the connection between two different axle groups, and the plus sign indicates the hitch connecting two vehicle units. Therefore, as shown in Fig 3.2, the TruckSim A-train model consists of a tractor, which has a front axle and a rear axle, two one-solid –axle trailers and a one-solid-axle dolly.

Figure 3.2. The configuration of the Trucksim model for A-Trains

3.3.2 Simulation Results Derived under a Single Lane-Change Maneuver

Tire corner stiffness is the most significant parameter needs to be determined when establishing the mathematic model. Different corner stiffness for tires may result in different results since tires are the most important nonlinear components directly determining the vehicle performance. Magic tire model is widely used in describing the characteristic of vehicle tires. The corner stiffness of a certain tire is associated with the

normal force and the slip angle of the tire. The normal force of each tire from first axle to fifth axle is 24400N, 15854N, 19164N, 15045N, 16870N respectively without longitudinal load transfer caused by longitudinal direction acceleration and lateral load transfer caused by lateral direction acceleration. For the slip angle, it is adequate to assume that the slip angle is less than 2 degree and the tires are still in linear region. It is justified by the TruckSim simulation result that the slip angle is less than 3 degree under the single-lane change maneuver specified by ISO-14791. The tire corner stiffness of the linear 5DOF yaw plane mathematic model is shown in appendix 2.

To validate the fidelity of the linear 5DOF yaw-plane model, the lateral performance of both the mathmatic model and the nonlinear TruckSim model are studied under the sine wave steering maneuver specified by ISO-14791 [24]. In this maneuver, the test vehicle is traveling at the forward speed of 88 km/h, and the tractor front axle wheel steer input is a single sine-wave with a frequency of 0.4 Hz and an adequate amplitude forcing the maximum lateral acceleration of the tractor to be around 0.15 g. Fig 3.3 shows the steer angle input of the tractor front axle wheel with an amplitude of 0.0194 rad.

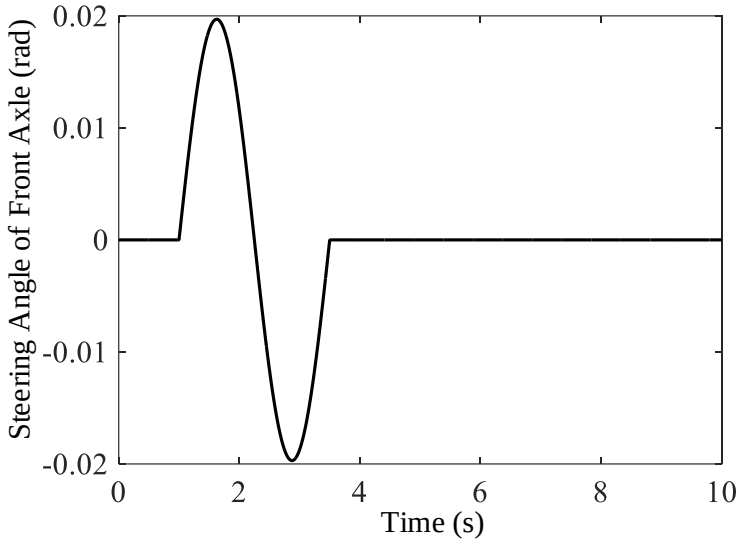

Figure 3.3. Time history of the steer angle input of the front axle wheel of the tractor of the A-Train

Figure 3.4 presents simulation results of the lateral accelerations for the 5 DOF yaw-plane model and the nonlinear TruckSim model. It is shown that under the simulation results of the two models derived under the same maneuver match well when the amplitude of lateral acceleration is not large enough to stimulate the nonlinear behaviors of the A-train double. The acceleration response from the linear model is symmetric along the axis resulted from symmetric wave disturbance input. In this situation, this A-train can be regarded as a linear model without losing any properties.

However, when the lateral acceleration starts to increase, the nonlinear performance of the A-train begins to take over, which makes the acceleration curves from the TruckSim model to have larger fluctuation than those of the linear model. This is easy to understand because the large acceleration will result in lateral load transfer making the corner stiffness of the

left tires and right tires differs. Beyond that, the roll motion will also add influences on the lateral dynamics.

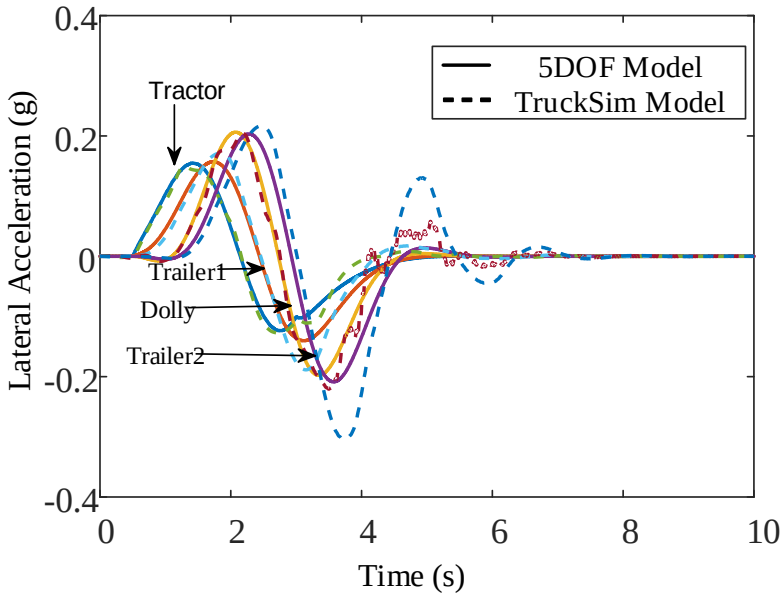

Figure 3.4. Time history of lateral acceleration of the 5 DOF yaw-plane model and the TruckSim model

The comparison of the time history of yaw rates of the 5 DOF yaw-plane model and the TruckSim model is shown in Fig 3.5. Curves of the tractor and the first trailer of both models are in good agreement. However, for the dolly and the second trailer, amplitudes of yaw rate curves of the TruckSim model are a little larger than those of the 5 DOF yaw-plane model.

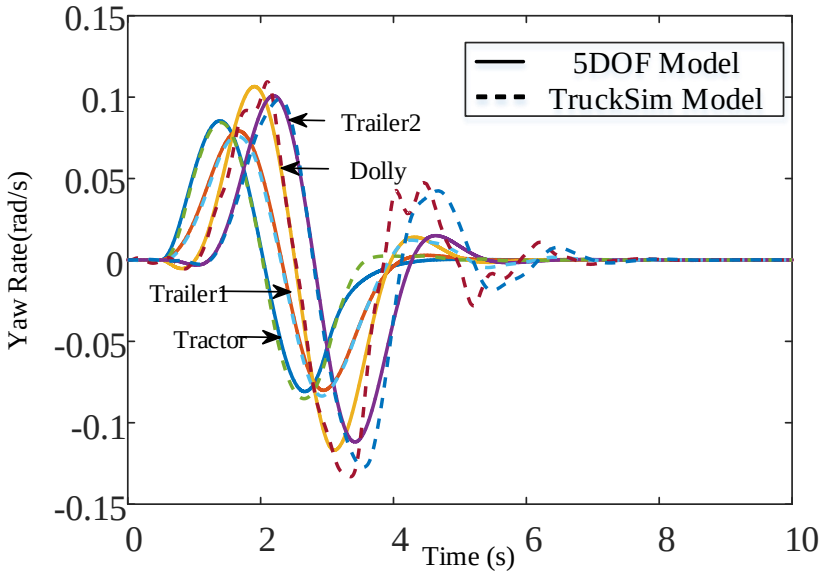

Figure 3.5. Time history of yaw rate of the 5 DOF yaw-plane model and the Trucksim model

Overall, the 5DOF yaw-plane model shows good agreement with the nonlinear TruckSim model in terms of lateral acceleration, yaw rate when the lateral acceleration is not too large. Even though these two models show some difference in high acceleration situation, the 5DOF yaw-plane model can still be used to design ATS controllers since it captures the main lateral behavior of the A-train double in highway speed. Moreover, to validate the ATS controller designed from employing the 5DOF yaw-plane model, the designed controller is needed to be tested again with the nonlinear TruckSim model or the hardware in loop platform to make the results more convincing.

Chapter 4

Test Maneuvers for Determining Lateral Dynamics

4.1 Introduction

RA has long been used as a good indicator for lateral stability and safety for multi-trailer articulated heavy vehicle at highway speeds. The International Organization for Standardization released the test maneuvers determining RA measure for LCVs in ISO-14791. ISO-14791 recommends two time domain methods and one frequency domain method to derive RA through experiments. The time-domain methods, e.g., an open-loop test procedure with a single sine-wave steering input, a driver closed-loop trajectory following method and the frequency-domain method, e.g. random steering wheel angle input method. However, some scholars have reported that the experiment test results from the three methods, however, differ in some degree. [John Aurell and Jacco Koppenaal, Ann Arbor, USA, 1995.].

To explore the contributing causes for this inconsistency among these methods, multiple cycle sine-wave steering input (MCSSI) maneuver is conducted in numerical simulation to obtain the steady lateral response of the LCVs. Furthermore, the automated frequency response method (AFRM) is conducted to validate the RA value measured from frequency

domain method. Simulation results demonstrate that the steady state RA measures of A-train double under MCSSI maneuver are in excellent agreement with the frequency domain methods. The transient response under time domain method imposes a non-neglected impact on the RA measures of A-train double.

4.2 Four Test Maneuvers Determining the RA Measures

For time domain methods, the lateral acceleration of each unit is measured under concerned frequency and thus obtaining the RA measure through the lateral accelerations of the tractor and rearmost trailer. The test is repeated under various frequency in time domain to derive the system gain in complete frequency domain. In view of the closed-loop trajectory following method, the test result is sensitive to the driver's preview time and response time. In frequency domain method, the LCV is regarded as a linear time-invariant (LTI) system, the system gain between the lateral accelerations of tractor and rearmost trailer is considered as RA measure of the LCV.

The first time domain maneuver is an open-loop test procedure with a single sine-wave steering input. One full period sinusoidal waveform steering angle is applied to the steering wheel following a period of neutral steering angle. The time history of the tractor's lateral acceleration is obtained which is close to a period of distorted sinusoidal waveform. The

test can be repeated at concerned frequency ranging from 0.1 Hz to 1 Hz in order to find out the maximum RA measure.

The second time domain maneuver is a closed-loop test procedure with a driver in the loop performed as a regulator to push the LCV following a predefined path. The path trajectory chosen for use in this procedure is designed corresponding to one full cycle of a sine wave of lateral acceleration. The test is repeated under different predefined paths to acquire the RA measures under different concerned frequency.

Random input maneuver is a frequency domain method by measuring the system gain between the tractor's acceleration and rearmost trailer's acceleration when vehicle's initial conditions and equilibrium point to be zero at certain test speed. This method can yield a whole representation of RA in full frequency domain.

The AFRM is another frequency domain test maneuver proposed by Zhu and He (2015). With the AFRM technique, the steer signal generation, vehicle excitation, and RA frequency function acquisition are conducted automatically at every frequency instantly. All the processes are completed before frequency being updated. This paper takes advantage of AFRM to validate the accuracy of RA measure in frequency domain derived from the numerical simulation.

In the process of all these test maneuvers, the vehicle's forward speed maintains constant at 88 km/h. An lateral acceleration amplitude of 0.15 g for the tractor is found reasonable level for investigating A-train double with RA around 2, since the maximum lateral acceleration of the rearmost trailer will be 0.3 g which is approaching the rollover threshold limit of many heavy trucks.

4.3 Numerical Simulation Result

4.3.1 Open-loop time domain method

Simulation results have shown that one full cycle of a sine wave steering angle input will lead to an asymmetric and distorted sinusoidal-like waveform of tractor's lateral acceleration, which making it difficult to quantify RA measure mathematically. In the draft ISO-14791, RA is recommended as the ratio between the maximum lateral acceleration of the rearmost trailer and tractor.

$$RA_{ISO} = \frac{\max(\left|a_{y\_trailer\_peak\_1}\right|, \left|a_{y\_trailer\_peak\_2}\right|)}{\max(\left|a_{y\_tractor\_peak\_1}\right|, \left|a_{y\_tractor\_peak\_2}\right|)} \tag{4.1}$$

The 0.4 Hz sine-wave steering wheel angle input is applied in the open-loop maneuver simulated in the numerical software. For A-train double under the open-loop maneuver, the Fig 4.1 (a), (b) and (d) show the time history of the lateral acceleration of each unit, the history of the yaw rate of each unit, and trajectories of the center of axles 1, 2, 4.

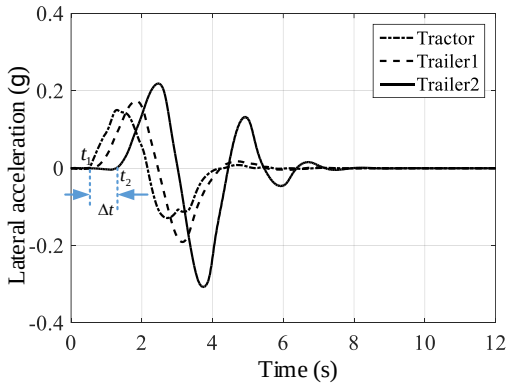

(a) Lateral acceleration

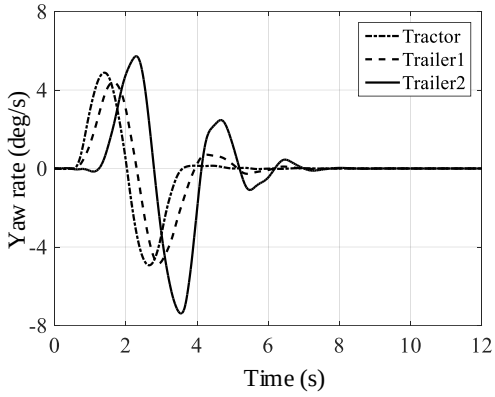

(b)Yaw rate

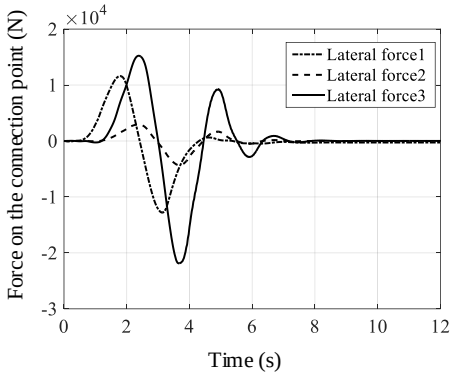

(c)Lateral force transmitted through

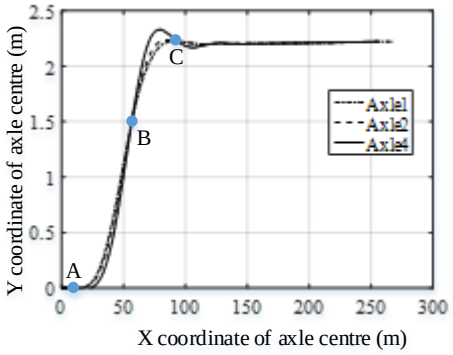

(d)Trajectory of each axle

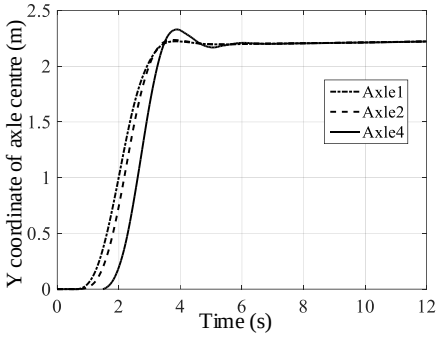

(e) Lateral movement of each axles

Figure 4.1. Time history of simulation result from open-loop test maneuver

There are five axles for A-train double in total. From the tractor front axle to the rearmost axle of trailer 2, they are denoted as axle1 to 5. The axle 1, 2, 4 are the front wheels for tractor, trailer1 and trailer2. The trailer1 is connected to the tractor by fifth wheel. The dolly is connected to the trailer 1 by hitch. The trailer 2 is connected to the dolly by fifth wheel as well.

As is shown in Fig4.1 (a), a 0.4 Hz sine waveform steering input is applied to the steering system at 0.5 s. The lateral acceleration of the tractor and yaw rate begin to increase at t_1 0.5 s. The lateral acceleration and yaw rate of the trailer 2 begin to increase at t_2 1.27 s. The time needed to transfer the lateral acceleration from the tractor to the rearmost trailer Δt is 0.76s. Therefore, the trailers do not response to the steering input immediately and are forced to perform lateral reaction through the lateral dragging force transmitted by the connection points. The lateral dragging forces on the connection points are shown in Fig4.1 (c). From the Fig4.1 (a) (b) (c), it is shown that the rearmost trailer trends to amplify and distort the lateral acceleration of the previous trailer or tractor with time delay. The rearmost trailer is more unstable than the tractor and is more likely to reach the rollover threshold limit even if the tractor is still in stable region.

As is shown in Fig 4.1(d), during the period of AB, the lateral displacement of Axle 4 is less than the lateral displacement of Axle 1 due to the acceleration transfer delay. The lateral displacement difference between Axle 4 and Axle 1 is decreasing which denotes

that the lateral acceleration of Axle 4 is larger than the lateral acceleration of Axle 1. During the period of BC, the lateral displacement of Axle 4 is large than that of Axle 1, which results in trailer 2 off-trajectory.

The positive peak lateral acceleration and peak yaw rate of the tractor are 0.15 g and 4.88 deg/s. The negative peak lateral acceleration at the tractor's gravity center is 0.128 g. The peak lateral acceleration and yaw rate of the rearmost trailer are 0.307 g and 7.38 deg/s. The final lateral displacement of axles 1, 2 and 4 are the same 2.2 m. Therefore, under 0.4 Hz sine wave steering input, the RA measure of the A-train double at 88 km/h is 2.21.

Repeat the test under different concerned frequency from 0.1 Hz to 1 Hz, the whole picture of the RA measures is shown in Fig 4.2

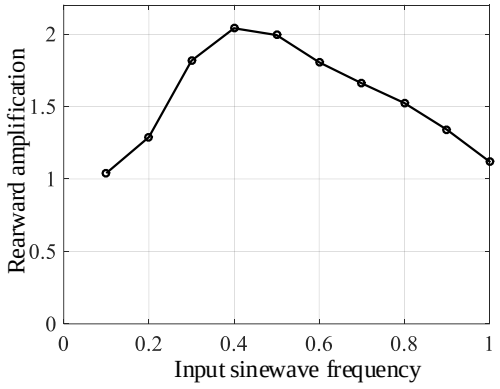

Figure4.2 RA measure under open-loop method

As is shown in Fig 4.2, the RA measured in open loop method get its maximum under 0.4 Hz sine-wave steering input. As is illustrated previously, the trailer 2 tends to obtain larger

lateral acceleration when the peak lateral acceleration of the tractor is kept the same 0.15 g. The lateral acceleration of the trailer 2 depends on the lateral force created by both the tires and fifth wheel. In order to illustrate why trailer 2 achieves maximum acceleration around 0.4 Hz steering, the articulated angle waveform of the trailer 2 is shown in Fig 4.3. The peak articulated angle of the trailer 2 under 0.4 Hz sine wave steering is larger than that under 0.1 Hz and 0.9 Hz sine wave steering. The maximum articulation angle for the trailer 2 reaches 2 degree under 0.4Hz steering. The large articulation angle will directly influence the lateral force transmitted to trailer 2 thus contributing to the peak value of the lateral acceleration for trailer 2.

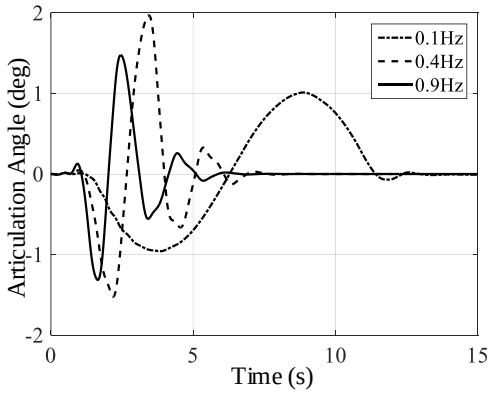

Figure4.3 Articulation angle of second fifth wheel under different frequency

4.3.2 Closed-loop Time Domain Maneuver

As is required in the ISO-14791, the LCVs shall follow a marked test course so that a selected point of tractor's the front axle does not deviate more than 0.15 m from the desired

path. It was found that with the aid of a sighting strip on the hood the driver could follow the path within this limit.

The test trajectory consists of a preliminary straight start section, an initial straight section, a single-lane maneuvering section and an exit section. The single-lane trajectory is defined by a kinematic relationship as

$$Y = \frac{a_{y1\_ax}}{(2\pi f)^2}\left[2\pi f \frac{X}{U_1} - \sin\left(2\pi f \frac{X}{U_1}\right)\right] \tag{4.2}$$

where f denotes the frequency of the lateral acceleration sine wave (Hz), U_1 is the forward velocity of the tractor unit (m/s), X is the longitudinal displacement, and Y denotes the lateral displacement of the test trajectory. The tractor's front axle center should be kept within 15 cm from the test trajectory during the test maneuvering. The simulation result is shown in Fig 4.4 under the trajectory designed for 0.4 Hz when the driver's preview time is chosen 0.12 s.

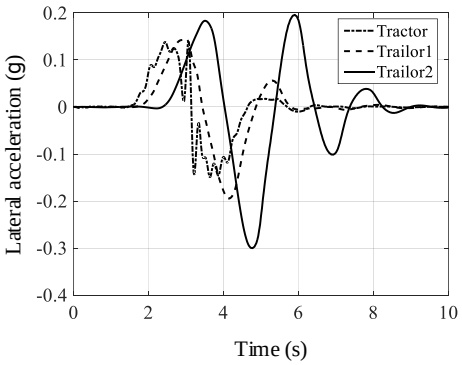

(a)Lateral acceleration

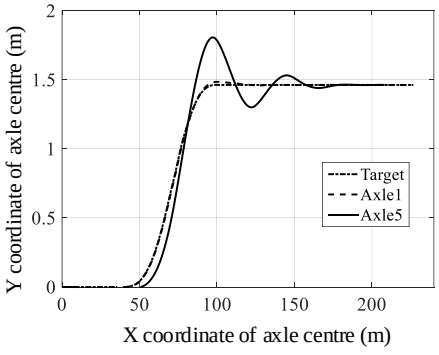

(b)trajectory of the axles

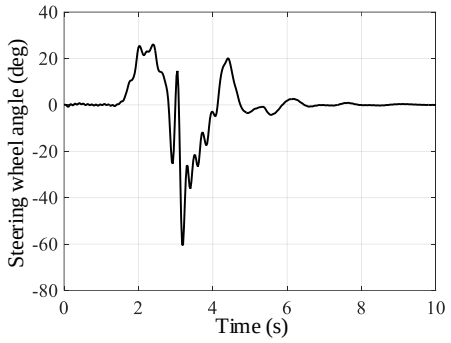

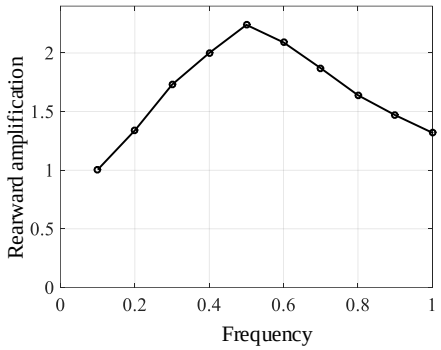

(c)Steering wheel angle (d)RA measures

Figure 4.4 Time history of simulation result from closed-loop Maneuver

As is shown in the Fig 4.4 (a), the peak lateral acceleration of the tractor is 0.15 g which is the same with that under the open-loop test maneuver. The maximum lateral deviation from the tractor axle's center point to the desire trajectory is 1.54 cm. The steering wheel angle of the driver is shown in Fig4.4 (c), which indicates that the driver in the loop performed as a real-time regulator to push the A-train following a predefined path. Repeat the test process under different designed trajectories, the RA derived from closed-loop method under 0.12 s preview time is shown in Fig4.4 (d). Considering the diversity of the drivers and the weather, the preview time of the driver may vary from 0.12 s to 1 s while keeping the trajectory tolerance band (TTB the maximum error distance between the center of the 1st axle and the desired target trajectory during the maneuvering) within the requirement of the ISO-14791. The RA measures obtained from closed-loop maneuver under different preview time are shown in Table 1.

Table 4.1 Closed-loop Lane Change Simulation Results under 0.4Hz

Preview time(s)	0.12	0.3	0.4	0.5	0.6	0.8	1
TTB(cm)	1.54	2.8	3.46	4.32	5.4	8.07	11.27
RA	2	2.17	2.1655	2.135	2.08	1.9827	1.8579

From the Table 4.1, the RA get its maximum under 0.3 s preview time with the TTB 2.8 cm. The RA values derived from trajectory following method are varying under different preview time and TTB distance. Even a small TTB distance difference may lead to unacceptable RA derivation and thus the accuracy of RA measure largely depends on the driver. As the preview time of the driver increases from 0.3 s to 1s, the TTB only increase no more than 9 cm. However, the RA decreases 14% from 2.17 to 1.8579 which is unacceptable for determining RA curve. All in all, the driver acted as a disturbance in the closed-loop test maneuver which imposes great influence on RA measure accuracy.

4.3.3 Random Steering Input Method

Random steering input method determining RA curve is a frequency domain method by measuring the system gain between the tractor's acceleration and rearmost trailer's acceleration when vehicle's equilibrium point to be zero at test speed. This method reveals the steady lateral characteristic of the A-train double and represents a whole picture of RA in frequency domain.

The steering angle input history is well designed considering the following four aspects: 1. the input steering angle time history should keep the vehicle in linear range during the maneuvering, 2. the steering input shall be energetic to make sure adequate high-frequency content. The frequency range of the steering input shall be from 0.1 Hz to as high as practicable but to at least 10 Hz considering the practical steering system. 3. Both the frequency and amplitude of the steering shall be varied randomly. It is also important that the input be continuous to reduce the signal/noise ratio. 4. To ensure enough total data, at least 12 min of the data is necessary to obtain the whole picture of the RA in frequency domain. In practice, the asymmetry of the steering system of A-train double will result in harmonic content of the input that cannot be eliminated. Random steering method has already taken adequate harmonic content of steering angle into consideration.

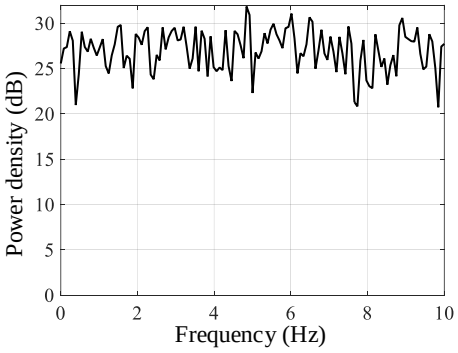

(a)power density of input steering angle

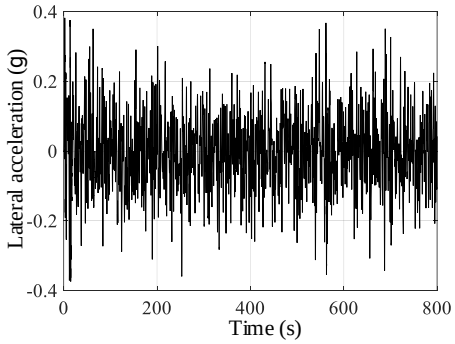

(b)lateral acceleration of trailer 2

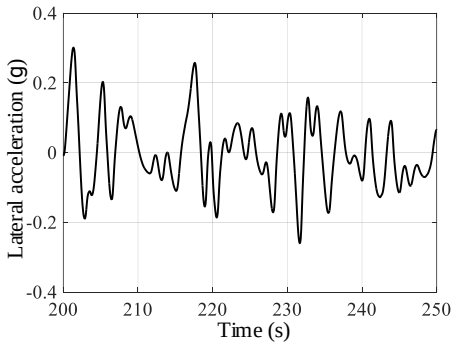

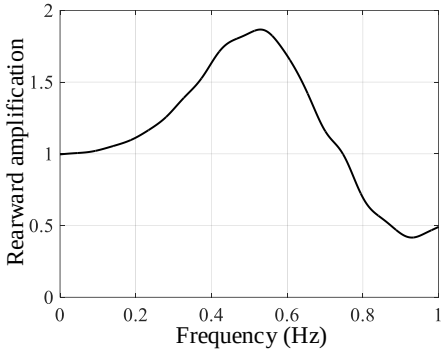

(c)lateral acceleration of trailer 2 (d)RA

Figure 4.5 Simulation results under Random input method

As is shown in Fig 4.5 (a), the steering angle input's power density is around 28 dB during the frequency from 0.1 Hz to 10 Hz. The whole test runs for 800 second to get an accurate value of the RA measurement. The RA curve derived through random input method is shown in Fig 4.5 (d), which shows a huge difference compared to the RA curves measured from two time domain methods.

4.3.4 Simulation Result under AFRM

In order to validate the accuracy of random input frequency domain method, another frequency domain method measuring RA is put forward as AFRM. In this method, the input steering angle is continuous sine-waveform with certain frequency interval to obtain the whole representation of the lateral acceleration response at certain speed. The cycle number of the sine waveform should be large enough to obtain the system gain between the tractor's and the second trailer's lateral accelerations.

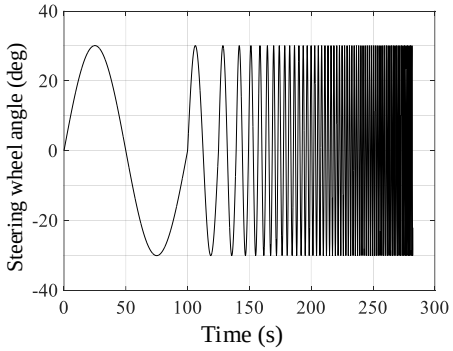

(a)Steering wheel angle

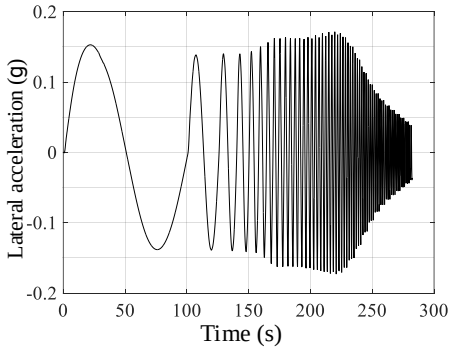

(b)Trailer2’s lateral acceleration

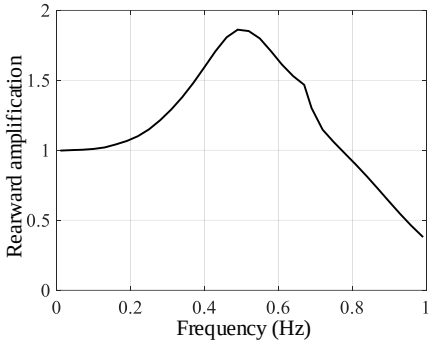

(c)RA curve

Figure 4.6 Simulation data from AFRM

Fig4.6 (a) shows that the input steering wheel angle is continuous sine waves with different frequency and different cycles. Fig4.6 (b) demonstrates the lateral acceleration of the trailer 2. The RA measure is calculated through Fourier transform of the lateral accelerations of the tractor and the trailer 2. The RA curve for A-train derived from AFRM is shown in Fig4.6 (c).

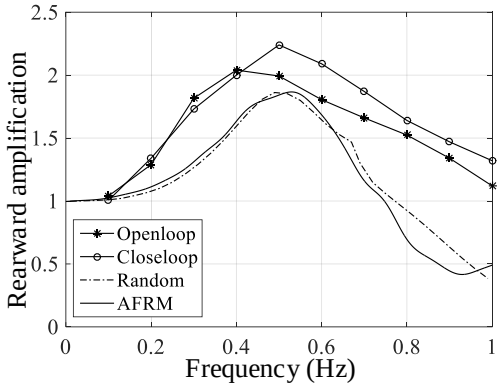

Figure 4.7 RWA obtained from different methods.

The RA curves derived from different test maneuvers are shown in Fig 4.7. Obviously, inconsistency exists between the time domain methods and frequency methods. Generally, the RA curves measured from time domain methods tend to be larger than those from frequency domain methods. And even for two time domain methods, the test results also differ in some degree. However, two frequency domain methods show good agreement with each other.

4.4 Comparison between Different Test maneuvers

As is shown in the Fig 4.7, by comparing the RA curves derived through open-loop and closed-loop methods, it appears that the RA derived from the driver closed-loop method tends to be larger than that from open-loop method. However, this is not always true since the driver's preview time is acted as a disturbance determining the RA curve under closed loop trajectory following method. Even if the preview time and TTB are varied within the requirement of ISO standards, the RA curves derived from closed-loop test maneuver still

show huge derivation as well. In this sense, even within a 15cm TTB requirement in test maneuvering, different driving characteristic may result in various steering angle waveforms applied into the steering system thus making RA curve obtained from closed-loop method uncertain in some degree.

Different drivers may perform different driving habits in following the designed trajectory which leads to different steering wheel input waveform all satisfying the requirement of ISO standards. As is shown in Fig 4.8, two steering wheel waveforms are acceptable for closed-loop test maneuver under trajectory designed for 0.4Hz.

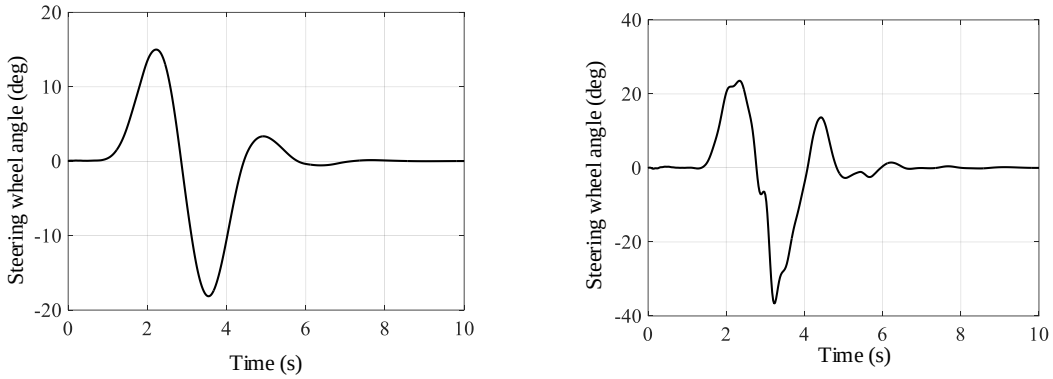

(a) (b)

Figure 4.8 Different driving behavior influences in closed-loop maneuvre

However, the RA derived from the Fig4.8 (a) steering strategy in close-loop testing method is 2.17 in 0.4 Hz case. Meanwhile the RA derived from the Fig4.8 (b) driving strategy is 1.86 in 0.4Hz case. Different driving habits impose non-neglected influences on steering

wheel input waveform and eventually instigate different level of transient response of the A-train lateral motion.

For two frequency testing methods, simulation results illustrate that within the concerned frequency range, RA derived from two methods achieve a good agreement. However, the RA curves obtained from time domain methods are different from those from frequency domain methods. In order to figure out the contributing causes to the inconsistency, MCSSI is applied to the steering wheel. For MCSSI method, as is shown in Fig 4.9 (a), 12 full cycles of 0.4 Hz sine waveform is applied into the steering wheel. The lateral acceleration time history waveforms at the center gravity of the tractor and trailer 2 are shown in Fig 4.9 (b) and Fig 4.9 (c).

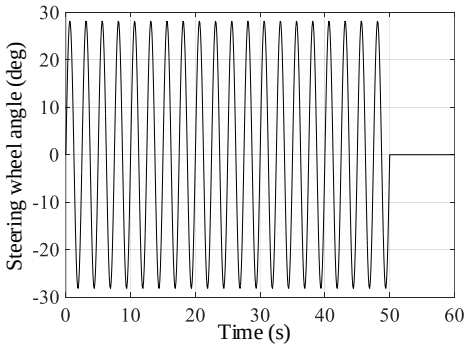

(a)steering wheel angle

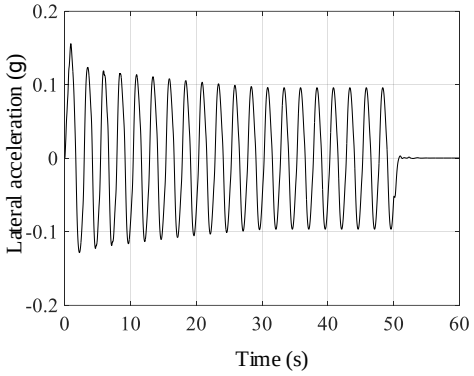

(b)acceleration of tractor

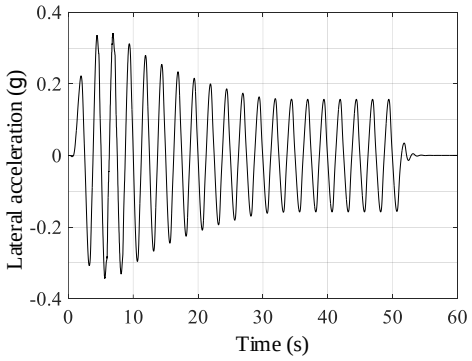

(c) acceleration of trailer 2

Figure 4.9 Time history of simulation result from MCSSI under 0.4Hz

The magnitude of tractor's lateral acceleration tends to decrease and then remains steady as the time passes by. The magnitude of the trailer 2's lateral acceleration gets maximum at third positive peak and then decreases until stable. The peak lateral acceleration values for tractor and trailer 2 are 0.153 g and 0.339 g respectively. The steady values for the counterparts are 0.096 g and 0.154 g. The RA measured from transient lateral acceleration and steady values are 2.216 and 1.6 respectively. Huge difference exists in determining RA by using transient lateral accelerations and steady lateral accelerations.

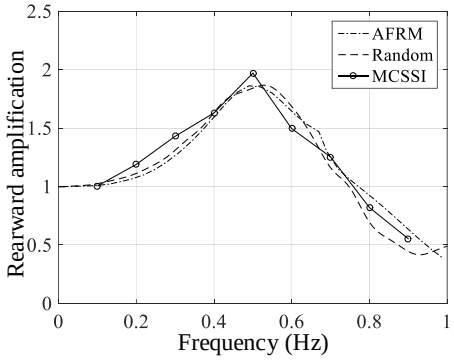

Figure 4.10 Steady RA from MCSSI

Taking advantage of the MCSSI results, the RA measures in lateral acceleration are calculated using the steady state values. The corresponding RA measured in MCSSI method is shown in Fig 4.10. It is noticeable that the steady RA curve derived from the MCSSI method shows good agreement with those from other two frequency domain methods.

Therefore, the random input frequency method and AFRM reveal the steady response of the A-train double lateral dynamic. However, two time domain methods take the transient response of the lateral dynamics into consideration. From this point, the RA curves measured from time domain methods include the transient response of the system thus making the RA measures tend to be larger than those from frequency domain methods.

Overall, simulation results derived from the research lead to the following insightful finding: 1) The RA value inconsistency between time domain and frequency domain methods mainly comes from the transient response of the LCVs in high speed. 2) For driver closed-loop trajectory following test method, different driving habits impose non-neglected influences on steering wheel input waveform and eventually instigate different level of transient lateral response of the LCVs. 3) The transient response of the lateral acceleration is diluted by increasing the cycles of the steering sine-waveform both in AFRM and MCSSI test methods.

Chapter 5

LQR Based ATS

5.1 Introduction

LQR theory is concerned with operating a dynamic system at minimum cost. The LQR problem can be reviewed as the weighted minimization of a linear combination of the states and the control inputs. The weighting matrix **Q** establishes which states are to be controlled more tightly than others. Matrix **R** adds weights to the control action to be applied depending on how large is the deviation of the states. This optimization cost weight constraints the magnitude of the control signal. LQR method seeks a controller that minimizes both energy of the controlled outputs and controlled signals.

5.2 LQR Controller Design

From the discussion from chapter 3, the 5DOF A-train double can be written in state-space form $\dot{x} = \mathbf{A}x + \mathbf{B}u$ by taking the driver's steering angle on the front axle δ as disturbance. For LQR ATS controller, the feedback gain matrix **K** is needed to be implemented as $u = -\mathbf{K}x$. The "A matrix" of the A-train double with ATS closed-loop system is therefore (**A-BK**).

5.2.1 LQR Theory

In the case of the LQR, the objective function is shown below,

$$\text{Choose } u(\text{t}) \text{ to minimize } \quad J = \int_0^\infty \frac{1}{2} x(t)^T \mathbf{Q} x(t) + \frac{1}{2} u(t)^T \mathbf{R} u(t) dt \tag{5.1}$$

$$\text{Subject to } \quad \dot{x} = f(x(t), u(t), t) = \mathbf{A}x + \mathbf{B}u$$

Take advantage of Lagrange multiplier λ(t), the augmented cost can be expressed as follow,

$$J = \int_0^\infty \frac{1}{2} x(t)^T \mathbf{Q} x(t) + \frac{1}{2} u(t)^T \mathbf{R} u(t) + \lambda^T (f - \dot{x}(t)) dt \tag{5.2}$$

Where both **Q** and **R** are positive definite matrices. To get the minimum value of objective function, partial derivative is applied to the objective function to get the extreme value.

$$\begin{cases} \dfrac{\partial J}{\partial u} = u^T \mathbf{R} + \lambda^T \mathbf{B} = 0 \\ \dfrac{\partial J}{\partial x} = x^T \mathbf{Q} + \lambda^T \mathbf{A} + \dot{\lambda}^T = 0 \end{cases} \tag{5.3}$$

Assume that $\lambda = \mathbf{P}x$, then insert into the equation,

$$\dot{\mathbf{P}}x + \mathbf{P}\dot{x} = -\mathbf{Q}x - \mathbf{A}^T \mathbf{P}x \tag{5.4}$$

Combined with the system state space model, the equation can be simplified as Riccati equation.

$$\mathbf{PA} + \mathbf{A^T P} + \mathbf{Q} - \mathbf{PBR^{-1}B^T P} = 0 \tag{5.5}$$

The matrix Riccati equation can be solved to find **P** through Hamiltonian matrix. Then the input *u* can be expressed as

$$u = -\mathbf{R}^{-1}\mathbf{B}^{\mathbf{T}}\mathbf{P}x \tag{5.6}$$

5.2.2 Solve Riccati Equation Based on Hamiltonian matrix

Define the following Hamiltonian matrix **H** as follow,

$$\mathbf{H} = \begin{bmatrix} \mathbf{A} & \mathbf{B}\mathbf{R}^{-1}\mathbf{B}^{\mathbf{T}} \\ \mathbf{R} & -\mathbf{A}^{\mathbf{T}} \end{bmatrix} \tag{5.7}$$

Let the column of $\begin{bmatrix} \mathbf{U}^{\mathbf{T}} & \mathbf{V}^{\mathbf{T}} \end{bmatrix}^{\mathbf{T}}, \mathbf{U}, \mathbf{V} \in \mathbb{R}^{n \times n}$, span n dimensional subspace of Hamiltonian matrix **H**,

$$\begin{bmatrix} \mathbf{A} & \mathbf{B}\mathbf{R}^{-1}\mathbf{B}^{\mathbf{T}} \\ \mathbf{R} & -\mathbf{A}^{\mathbf{T}} \end{bmatrix} \begin{bmatrix} \mathbf{U} \\ \mathbf{V} \end{bmatrix} = \begin{bmatrix} \mathbf{U} \\ \mathbf{V} \end{bmatrix} \mathbf{Z}, \mathbf{Z} \in \mathbb{R}^{n \times n} \tag{5.8}$$

Assuming that **U** is nonsingular, the first row is simplified

$$\mathbf{U}^{-1}\mathbf{A}\mathbf{U} + \mathbf{U}^{-1}\mathbf{B}\mathbf{R}^{-1}\mathbf{B}^{\mathbf{T}}\mathbf{V} = \mathbf{Z} \tag{5.9}$$

Combined with the second row equation

$$\mathbf{R}\mathbf{U} - \mathbf{A}^{\mathbf{T}}\mathbf{V} = \mathbf{V}\left(\mathbf{U}^{-1}\mathbf{A}\mathbf{U}^{\mathbf{T}} + \mathbf{U}^{-1}\mathbf{B}\mathbf{R}^{-1}\mathbf{B}^{\mathbf{T}}\mathbf{V}\right) \tag{5.10}$$

$$\mathbf{R} - \mathbf{A}^{\mathbf{T}}\mathbf{V}\mathbf{U}^{-1} - \mathbf{V}\mathbf{U}^{-1}\mathbf{A} - \mathbf{V}\mathbf{U}^{-1}\mathbf{B}\mathbf{R}^{-1}\mathbf{B}^{\mathbf{T}}\mathbf{V}\mathbf{U}^{-1} = \mathbf{0} \tag{5.11}$$

Setting $\mathbf{X} = \mathbf{V}\mathbf{U}^{-1}$, the equation the same as Riccati equation. Therefore, the Riccati equation can be easily solved by Hamiltonian matrix composition.

5.3 Parameter Robust Analysis of ATS

5.3.1 Mathematic Model with Parameter Robust

To date, the LQR technique has mainly been applied to designing controllers for ATS systems of AHVs. However, these LQR controllers were designed under the assumption that the vehicle model parameters and operating conditions were given and they remained as constants. In reality, the vehicle system parameters, operating conditions, as well as external disturbances may vary. Here the forward speed U is chosen as a parameter uncertainty and changes in a certain range $U \in [U_{\min} \quad U_{\max}]$. Then the system matrix can be expressed as follow, in which it is interesting to reveal that $\mathbf{B_u}$ matrix does not change with the forward speed U in 5DOF mathematic model of A-train.

$$\dot{x} = \mathbf{A}(U)x + \mathbf{B_u}u \quad U \in [U_{\min} \quad U_{\max}] \tag{5.12}$$

The Fig 5.1 shows the ATS experimental test bed in UOIT, the third axle of A-train double is chosen to be an active steering axle. The hardware in loop ATS takes advantage of an electric actuator to steer the axle to the desired angle. The angle sensor is installed on the axle to realize steering angle closed-loop control.

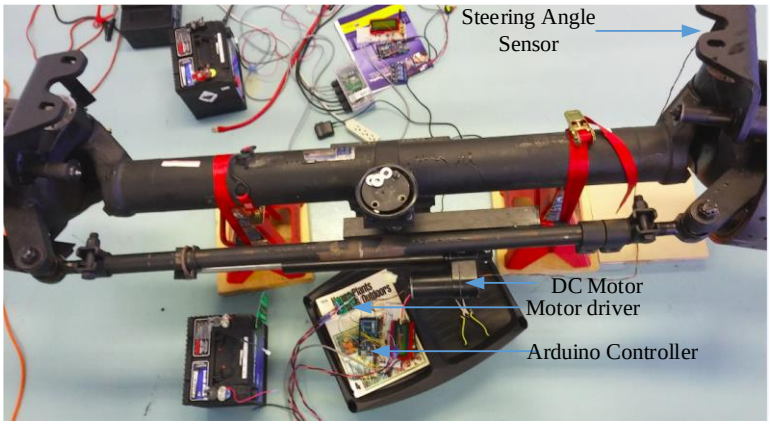

Figure 5.1 ATS Experimental Test Bed

The steering angle sensor feeds back the actual steering angle into the Arduino chip. The demanded steering angle is calculated through Labview. The Arduino sends out the steering speed information of the active axle to the actuator controller by taking advantage of error between the demanded steering angle and actual angle of the active axle. Proportional–integral–derivative (PID) algorithm is programmed in Arduino to manipulate the electric actuator's steering speed. Serial communication is used in the Arduino chip to send out the steering speed of the active axle to the steering controller. The speed control word for the actuator is 0x89 and 0x139 and the speed parameter ranges from 0 to 128 according to the Pololu Corporation [37].

According to [38], the steering angle closed-loop electric active steering axle can be simplified as the following mathematic model,

$$G_a = \frac{1}{T_a s + 1} \quad T_a \in [T_{a\min} \quad T_{a\max}] \tag{5.13}$$

The parameter T_a depends on the performance of the steering system. If the actuator can response quickly to the steering angle input, T_a could be small enough. Otherwise, T_a could be very large when the actuator steering speed is low.

Above all, the mathematic model of the A-train double with ATS is shown in Fig 5.2, in which u_1 is the output demanded steering angle of the ATS controller, u is real feedback angle of the active axle.

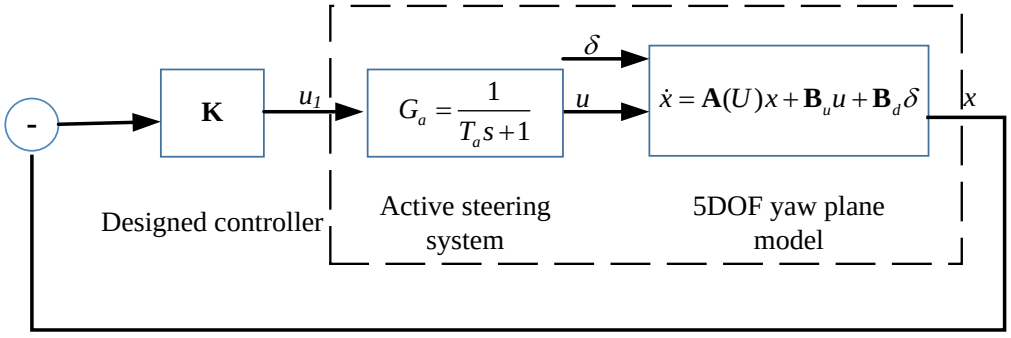

Figure 5.2 Mathematic Model for A-train considering the ATS

The mathematic model of the A-train combined with active steering axle can be summary as follow,

$$\dot{x} = \mathbf{A}(U)x + \mathbf{B}_u u + \mathbf{B}_d \delta \tag{5.14}$$

$$\dot{u} = -\frac{1}{T_a}u + \frac{1}{T_a}u_1 \tag{5.15}$$

$$y = Cx + Du \tag{5.16}$$

Then the augmented matrices $\bar{\mathbf{A}}(U, T_a)$, $\bar{\mathbf{B}}_{\mathbf{u}}(T_a)$, $\bar{\mathbf{C}}$ of the state space model considering the ATS are shown as follow,

$$\begin{bmatrix} \dot{x} \\ \dot{u} \end{bmatrix} = \begin{bmatrix} \mathbf{A}(U) & \mathbf{B}_u \\ \mathbf{0} & -\frac{1}{T_a} \end{bmatrix} \begin{bmatrix} x \\ u \end{bmatrix} + \begin{bmatrix} \mathbf{0} \\ \frac{1}{T_a} \end{bmatrix} u_1 + \begin{bmatrix} \mathbf{B}_d \\ 0 \end{bmatrix} \delta \tag{5.17}$$

$$y = \begin{bmatrix} C & D \end{bmatrix} \begin{bmatrix} x \\ u \end{bmatrix} \tag{5.18}$$

$$U \in [U_{\min} \quad U_{\max}] \quad T_a \in [T_{a\min} \quad T_{a\max}] \tag{5.19}$$

5.3.2 Robust analysis of conventional LQR controller

LQR controllers are inherently robust with respect to process uncertainty. To analysis the robust characteristic of the conventional LQR method for ATS of A-train, the open loop diagram of the closed-loop system can be expressed in Fig 5.3,

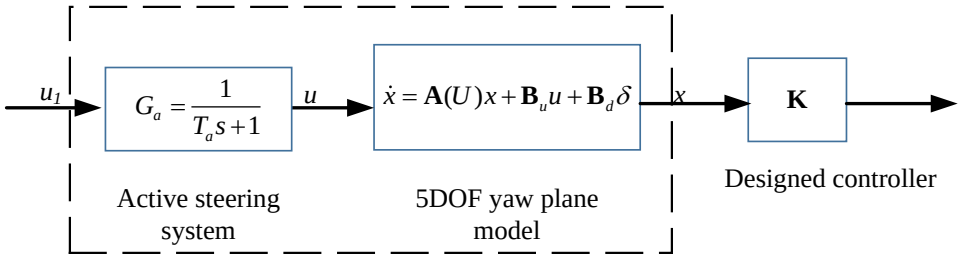

Figure 5.3 Open Loop of the LQR Closed-loop System

The open loop negative feedback gain is shown as follow,

$$G_0(s) = \mathbf{K}(\mathbf{sI} - \bar{\mathbf{A}}(U, T_a))^{-1} \bar{\mathbf{B}}_{\mathbf{u}}(T_a) \tag{5.20}$$

From the Kalman's inequality [37], the Nyquist plot of G_0(j ω) does not enter a circle of radius one around -1. That is

$$\left|1 + G_0(j\omega)\right| > 1 \tag{5.21}$$

From the Kalman's inequality, the closed-loop system with such LQR controller presents interesting properties like a phase margin larger than 60 degree and infinite gain margin.

The augmented system matrix $\bar{\mathbf{A}}(U,T_a)$ depends on forward velocity and active steering system parameter T_a. The Input matrix $\bar{\mathbf{B}}_{\mathbf{u}}(\beta)$ depends on the active steering system parameter β=1/T_a. These elements involved in the system matrices are uncertain or time varying. Then the augmented model is written in state space model as

$$\dot{x} = \bar{\mathbf{A}}(U,T_a)x + \bar{\mathbf{B}}_u(\beta)u \tag{5.22}$$

For further analysis the stability of LQR feedback system, Lyapunov's theory is applied to the system, a useful analogy for the Lyapunov function is energy, dissipated in a passive mechanical system by damping, or in a passive electrical system through resistance. The details of Lynapunov's theory is referred to [39-42]. The following lemma illustrates the quadratical stability of the closed-loop A-train system with ATS controller.

Lemma 5.1: A constant state feedback matrix **K** can be used to obtain quadratical stability for varying velocity by exploiting the convex nature of the lateral dynamic system. The constant feedback matrix **K** will stabilize the system for the speed range $U \in [U_{\min} \quad U_{\max}]$ iif:

$$\begin{cases} \bar{\mathbf{A}}_{\mathbf{cl}}^{\mathbf{T}}(U_{\min},T_a,\beta)\mathbf{P} + \mathbf{P}\bar{\mathbf{A}}_{\mathbf{cl}}(U_{\min},T_a,\beta) < 0 \\ \bar{\mathbf{A}}_{\mathbf{cl}}^{\mathbf{T}}(U_{\max},T_a,\beta)\mathbf{P} + \mathbf{P}\bar{\mathbf{A}}_{\mathbf{cl}}(U_{\max},T_a,\beta) < 0 \end{cases} \tag{5.23}$$

Where, **P**>0 and the closed-loop matrix $\bar{\mathbf{A}}_{\mathbf{cl}}(U,T_a,\beta)$ can be defined as

$$\bar{\mathbf{A}}_{\mathbf{cl}}(U,T_a,\beta)=\bar{\mathbf{A}}(U,T_a)-\bar{\mathbf{B}}_{\mathbf{u}}(\beta)\mathbf{K} \tag{5.24}$$

From the Lemma 5.1, if constant feedback **K** stabilize the plant under both maximum and minimum speeds, then feedback matrix **K** will also stabilize all the possible speed during the range between [41].

For any active steering axle parameter $T_a \in [T_{a\min} \quad T_{a\max}]$, it is also available to exploit the convex property of the $\bar{\mathbf{A}}_{\mathbf{cl}}(U,T_a,\beta)$ matrix due to its special structure.

$$\bar{\mathbf{A}}_{\mathbf{cl}}(U,T_a,\beta)=a\bar{\mathbf{A}}_{\mathbf{cl}}(U,T_{a\min},\beta)+(1-a)\bar{\mathbf{A}}_{\mathbf{cl}}(U,T_{a\max},\beta) \qquad a\in\begin{bmatrix}0 & 1\end{bmatrix} \tag{5.25}$$

Taking advantage of the Lyapunov's theory, the feedback **K** feedback stabilizes the system considering the parameter robust of T_a, iif

$$\begin{cases}\mathbf{A}_{\mathbf{cl}}^{\mathbf{T}}(U,T_{a\min},\beta)\mathbf{P}+\mathbf{P}\mathbf{A}_{\mathbf{cl}}(U,T_{a\min},\beta)<0\\ \mathbf{A}_{\mathbf{cl}}^{\mathbf{T}}(U,T_{a\max},\beta)\mathbf{P}+\mathbf{P}\mathbf{A}_{\mathbf{cl}}(U,T_{a\max},\beta)<0\end{cases} \tag{5.26}$$

The similar inequalities can be obtained for parameter $\beta\in[\beta_{\min} \quad \beta_{\max}]$. In conclusion, due to the convex property of the system matrix, the chosen of the feedback matrix **K** should satisfy the 2^3 LMIs in order to take the parameter uncertainties forward speed U and active axle parameter T_a into consideration. A convex solution set has no hidden corners or shadows, because every point on a straight line between two solutions is also a solution. Therefore, the robust analysis of LQR controller is a convex optimization problem.

5.4 ATS Design Based on LQR

In this section, conventional LQR method and LQR-LMI robust control with GA are applied to the A-train. Both the simulation results of the A-train under two designed controllers are obtained. The ATS controller is validated in UOIT vehicle simulation platform shown in Fig 5.4. The UOIT vehicle simulator consists of a host computer, an animator computer, a LABVIEW real-time computer. These units are connected by a controller area network and Ethernet network. The host computer is installed with the TruckSim to define and compile the real-time A-train model. The LQR controller is reconstructed in LabVIEW-RT model to implement hardware in loop real-time simulation.

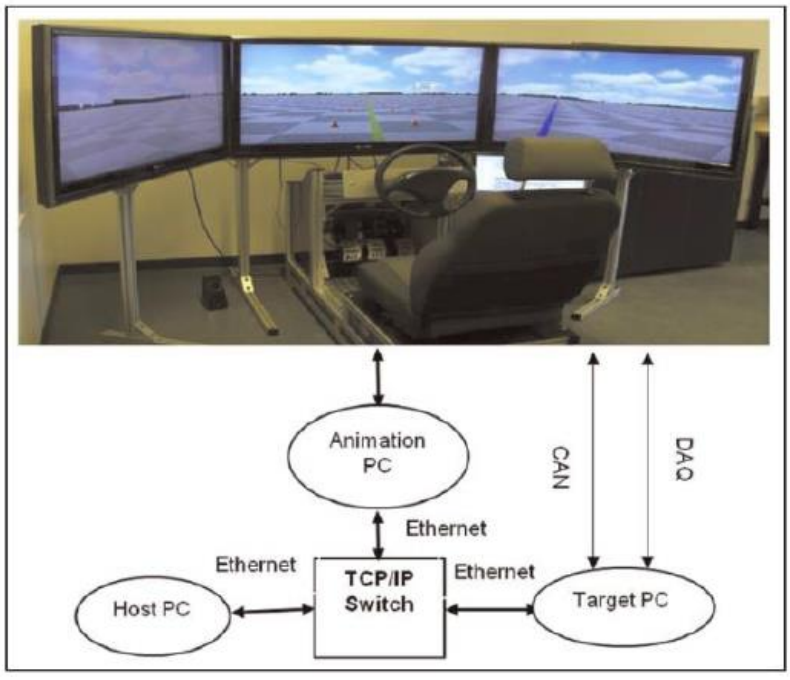

Figure 5.4 System architecture of the UOIT vehicle simulator

5.4.1 Conventional LQR Method for ATS

As is illustrated previously, the conventional LQR is an optimization method through the whole time domain for the designed case. The ATS controller for the A-train double is designed via conventional LQR method. The weights of the performance index matrices **Q** and **R** are chosen such that the RA of the train reduces with minimum active steering angle effort. The pair of **Q** and **R** is designed for A-train in the designed case with forward speed U=88 km/h and active axle parameter T_a=1.5 s. The conventional LQR ATS controller for the plant can be designed under the toolbox of Matlab lqr command. The LQR ATS controller designed from Matlab is run with TruckSim model. The driver's steering angle of front axle in the tractor is shown in Fig 5.5, it is a sine waveform steering.

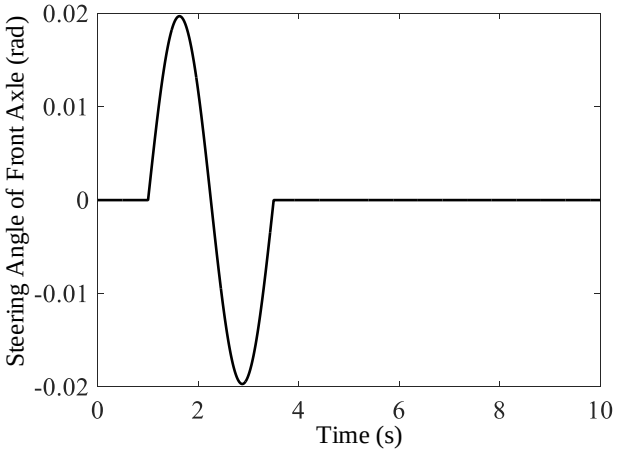

Figure 5.5 steer angle input of the front axle wheel of the tractor of the A-Train

The performance of the A-train without ATS is shown in Fig 5.6 at different forward speeds 68 km/h, 88 km/h and 108 km/h respectively. The lateral acceleration of the 2nd trailer

increases as the forward speed rises. The acceleration of 2nd trailer reaches nearly 0.4 g under 108 km/h forward speed, which is a dangerous case.

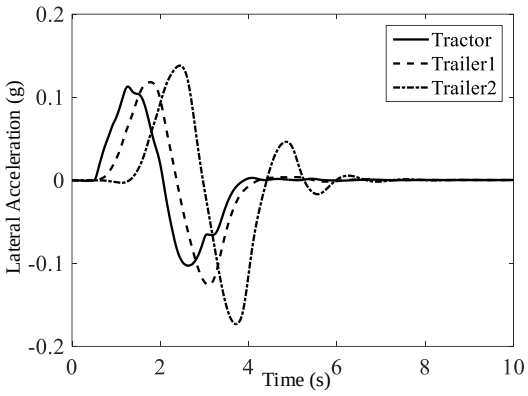

(a)68 km/h

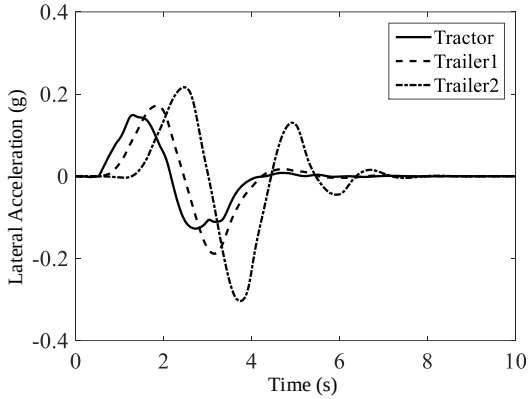

(b)88 km/h

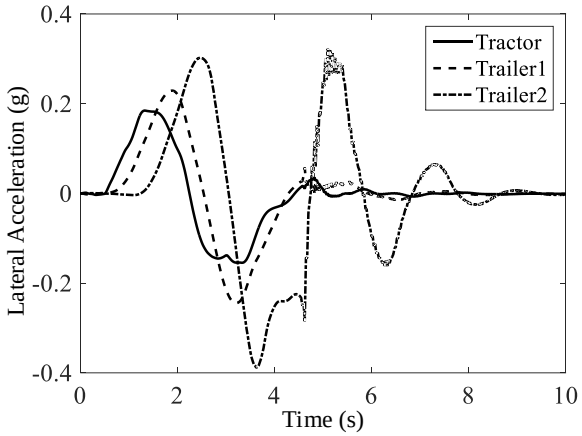

(c)108 km/h

Figure 5.6 Performance of the A-train under different forward speed

The conventional LQR controller is designed and applied to the third axle of the A-train double. The steering angle waveform of the front axle remains the same in the following test maneuvers under different active axle time parameters. The lateral acceleration waveforms of the tractor and two trailers are shown in Fig 5.7.

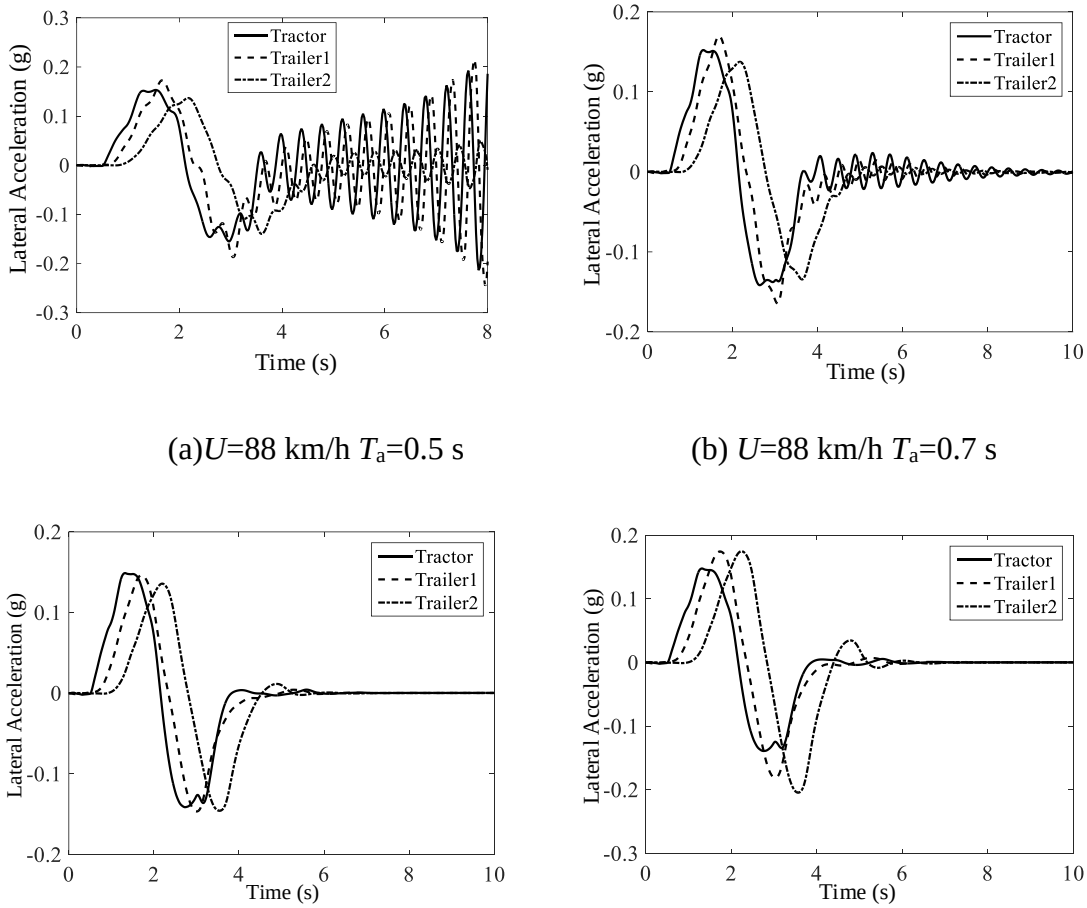

(a)U=88 km/h T_a=0.5 s (b) U=88 km/h T_a=0.7 s

(c)U=88 km/h T_a=1.5 s (d)U=88 km/h T_a=2.5 s

Fig 5.7 Performance of the A-train under LQR with different time parameters

The peak lateral acceleration of rearmost trailer decreases from 0.307 g to 0.156 g compared to counterpart in the Fig 5.6 under 88km/h forward speed and 1.5s axle time parameter, which means that the LQR ATS controller works well for this designed case. And the lateral acceleration of 2nd trailer inclines to rise up with the increasing of the active axle parameter T_a because the response speed of the axle decreases. However, it is interesting to find out that the control system will lose stability when T_a is less than 0.7 s, which reveals that the LQR ATS controller designed under parameter T_a 1.5 s is not suitable

for the active steering axle whose time parameter T_a less than 0.7 s. This is understandable since the conventional LQR doesn't take the parameter uncertainty into consideration.

The time parameter of the active axle remains to be 1.5 s. The forward speed of the A-train double varies from 68 km/h to 108 km/h. The performance of the tractor and trailers with the LQR ATS controller designed for 88 km/h forward speed and 1.5 s active axle time parameter is shown in Fig 5.8.

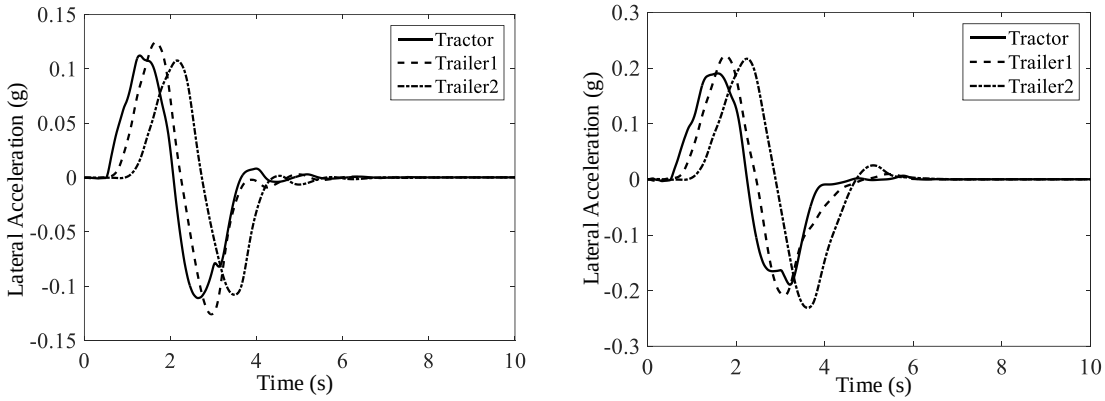

(a)U=68 km/h T_a=1.5 s (b)U=108 km/h T_a=1.5 s

Figure 5.8 Performance of A-train with LQR controller under different speed

When the forward speed is 68km/h, the rearmost trailer's peak lateral acceleration decreases from 0.176 g to 0.106 g. The peak lateral acceleration of the rearmost trailer decreases from 0.397 g to 0.235 g under 108 km/h case.

Therefore, the conventional LQR method may result in good results at designed case. However, it doesn't take the parameter variation into consideration. For example, the active axle time parameter T_a, it will vary with time because the time parameter even for the same active steering axle differs under different loads of the train and different control methods

of steering actuator. Beyond that, the forward speed is impossible to be kept as a constant when the train is performing single lane change maneuvering. To achieve parameter robust for the controller, the robust LQR-LMI method with GA optimization is put forward.

5.4.2 LQR-LMI Robust Method with GA Optimization

The LQR problem can also be formulated in form of linear matrix inequalities (LMI), and numerically solved by convex optimization method. A linear control design method based on LQR is presented, in which we achieve robust stability despite model inaccuracies. The formation of the LQR problem, adapted from [43] [44].

The optimal LQR controller is obtained by using the state-feedback gain **K** that minimizes a performance index *J*. For the closed-loop, the performance index is rewritten

$$\begin{aligned} J &= \int_0^\infty (x^T \mathbf{Q} x + u^T \mathbf{R} u) dt \\ &= \int_0^\infty x^T (\mathbf{Q} + \mathbf{K}^\mathbf{T} \mathbf{R} \mathbf{K}) x dt \\ &= \mathbf{Tr}((\mathbf{Q} + \mathbf{K}^\mathbf{T} \mathbf{R} \mathbf{K}) \mathbf{P}) \end{aligned} \tag{5.27}$$

Tr( ) is the trace operator. And $\mathbf{P} = \int_0^\infty x(t)x(t)^T dt$ is a definite positive symmetric matrix. From the time-domain solution of LTI state equations [45], the system homogeneous response may be written in terms of the matrix exponential $x(t) = e^{(\bar{\mathbf{A}}\text{-}\bar{\mathbf{B}}_\mathbf{u}\mathbf{K})t} x(0)$, then

$$
\begin{aligned}
(\bar{\mathbf{A}}-\bar{\mathbf{B}}_{\mathbf{u}}\mathbf{K})\mathbf{P}+\mathbf{P}(\bar{\mathbf{A}}-\bar{\mathbf{B}}_{\mathbf{u}}\mathbf{K})^{\mathbf{T}} &= \lim_{t\to\infty}\int_0^t (\bar{\mathbf{A}}-\bar{\mathbf{B}}_{\mathbf{u}}\mathbf{K})e^{(\bar{\mathbf{A}}-\bar{\mathbf{B}}_{\mathbf{u}}\mathbf{K})t}x(0)x(0)^{\mathbf{T}}e^{(\bar{\mathbf{A}}-\bar{\mathbf{B}}_{\mathbf{u}}\mathbf{K})^{\mathbf{T}}t} + \\
&\quad e^{(\bar{\mathbf{A}}-\bar{\mathbf{B}}_{\mathbf{u}}\mathbf{K})t}x(0)x(0)^{\mathbf{T}}e^{(\bar{\mathbf{A}}-\bar{\mathbf{B}}_{\mathbf{u}}\mathbf{K})^{\mathbf{T}}t}(\bar{\mathbf{A}}-\bar{\mathbf{B}}_{\mathbf{u}}\mathbf{K})^{\mathbf{T}}dt \\
&= \lim_{t\to\infty}(e^{(\bar{\mathbf{A}}-\bar{\mathbf{B}}_{\mathbf{u}}\mathbf{K})t}x(0)x(0)^{\mathbf{T}}e^{(\bar{\mathbf{A}}-\bar{\mathbf{B}}_{\mathbf{u}}\mathbf{K})^{\mathbf{T}}t})_0^t
\end{aligned}
\tag{5.28}
$$

By using the cyclic property of the trace, which satisfies **Tr**(XY)=**Tr**(YX). The optimal feedback gain **K** from LQR method can be found by minimization of the following expression

$$
\min_{\mathbf{K},\mathbf{P}} \mathbf{Tr}(\mathbf{QP})+\mathbf{Tr}(\mathbf{R}^{\frac{1}{2}}\mathbf{K}\mathbf{P}\mathbf{K}^{\mathbf{T}}\mathbf{R}^{\frac{1}{2}})
\tag{5.29}
$$

$$
\text{Subject to} \quad \bar{\mathbf{A}}\mathbf{P}+\mathbf{P}\bar{\mathbf{A}}^{\mathbf{T}}-\bar{\mathbf{B}}_{\mathbf{u}}\mathbf{Y}-\mathbf{Y}\bar{\mathbf{B}}_{\mathbf{u}}<0
$$

By defining a new quantity$\mathbf{Y}=\mathbf{KP}$, the above problem can be rewrite as follow [42-43],

$$
\min_{\mathbf{P},\mathbf{K}} \mathbf{Tr}(\mathbf{QP})+\mathbf{Tr}(\mathbf{X})
$$

$$
\begin{aligned}
&\bar{\mathbf{A}}\mathbf{P}+\mathbf{P}\bar{\mathbf{A}}^{\mathbf{T}}-\bar{\mathbf{B}}_{\mathbf{u}}\mathbf{Y}-\mathbf{Y}^{\mathbf{T}}\bar{\mathbf{B}}_{\mathbf{u}}^{\mathbf{T}}<0 \\
&\text{Subject to} \begin{bmatrix} \mathbf{X} & \mathbf{R}^{\frac{1}{2}}\mathbf{Y} \\ \mathbf{Y}^{\mathbf{T}}\mathbf{R}^{\frac{1}{2}} & \mathbf{P} \end{bmatrix}>0 \quad \mathbf{P}>0
\end{aligned}
\tag{5.30}
$$

This is a convex non-differentiable optimization program, and the ellipsoid algorithm or Kelley's cutting-plane algorithm can be applied to solve it. Then the feedback controller can be recovered by $\mathbf{K}=\mathbf{YP}^{-1}$.

Therefore, the robust LQR control solved via LMIs is a convex optimization problem. For the A-train case, forward speed (km/h) $U\in[68 \quad 108]$ and the actuator parameter (s)

$T_a \in [0.5 \quad 2.5]$ are considered as variable uncertainties. The 3rd axle is chosen to be the active steering axle in the A-train. By taking advantage of the convex nature of the system to deal with the modeling uncertainty, the matrices $\bar{\mathbf{A}}$ and $\bar{\mathbf{B}}_{\mathbf{u}}$ in (5.30) can be substituted by the vertices of the $\bar{\mathbf{A}}(U, T_a)$ and $\bar{\mathbf{B}}_{\mathbf{u}}(\beta)$ similar to the inequalities listed in (5.23) and (5.26).

The GA is introduced to optimize index matrices **Q** and **R** of the LQR-LMI controller. GA is a search heuristic method that mimics the procedures of natural selection, which generates solutions to optimization problems using natural evolution. The candidate solution is searched in solution domain by mutation, inheritance, selection and crossover. And a fitness function is defined to evaluate the candidate solution. As is illustrated before, the index matrices **Q** and **R** are both needed in LQR-LMI convex optimization method to calculate the feedback matrix **K**. Therefore, the proposed method combines GA and LQR-LMI convex optimization method. The GA deals with searching appropriate matrices **Q** and **R** while convex optimization method copes with calculating feedback matrix **K** with certain parameter robust. The program flow diagram of the robust LQR-LMI-GA method is illustrated in Fig 5.9.

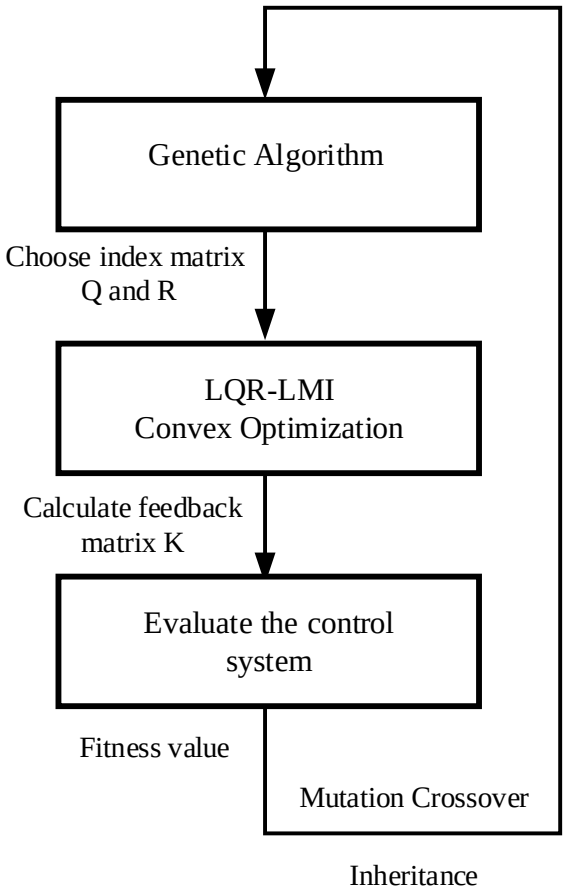

Figure 5.9 Program flow of LQR-LMI method with GA

When designing the LQR-LMI controller for A-train double, the choice of fitness function for GA is of great significance. In order to obtain better RA curves for closed-loop A-train double, the fitness function of GA is chosen as

$$F = \sum_{i=1}^{4} \frac{\max(|\bar{a}_i|)}{rms(a_i)} + \frac{rms(\bar{r}_i)}{rms(r_i)} \tag{5.31}$$

Where $\bar{a}_i$ (i=1, 2, 3, 4) and $\bar{r}_i$ (i=1, 2, 3, 4) are the lateral acceleration and yaw rate of tractor, 1st trailer, dolly and 2st trailer respectively with ATS controller designed via robust LQR-LMI method. Meanwhile a_i and r_i are the counterparts of the A-train double

without ATS controller. The corresponding feedback matrix **K** designed by robust LQR-LMI algorithm with GA optimization is shown in below,

$$K = \begin{bmatrix} 2.43 & -15.74 & 1.51 & -39.44 & -3.52 & 3.00 & -1.16 & -2.88 & 126.14 \end{bmatrix} \quad (5.32)$$

The steering waveform of the driver is the same as Fig 5.5. The lateral accelerations of the tractor and two trailers under the designed ATS controller are shown in Fig 5.10 at different speeds.

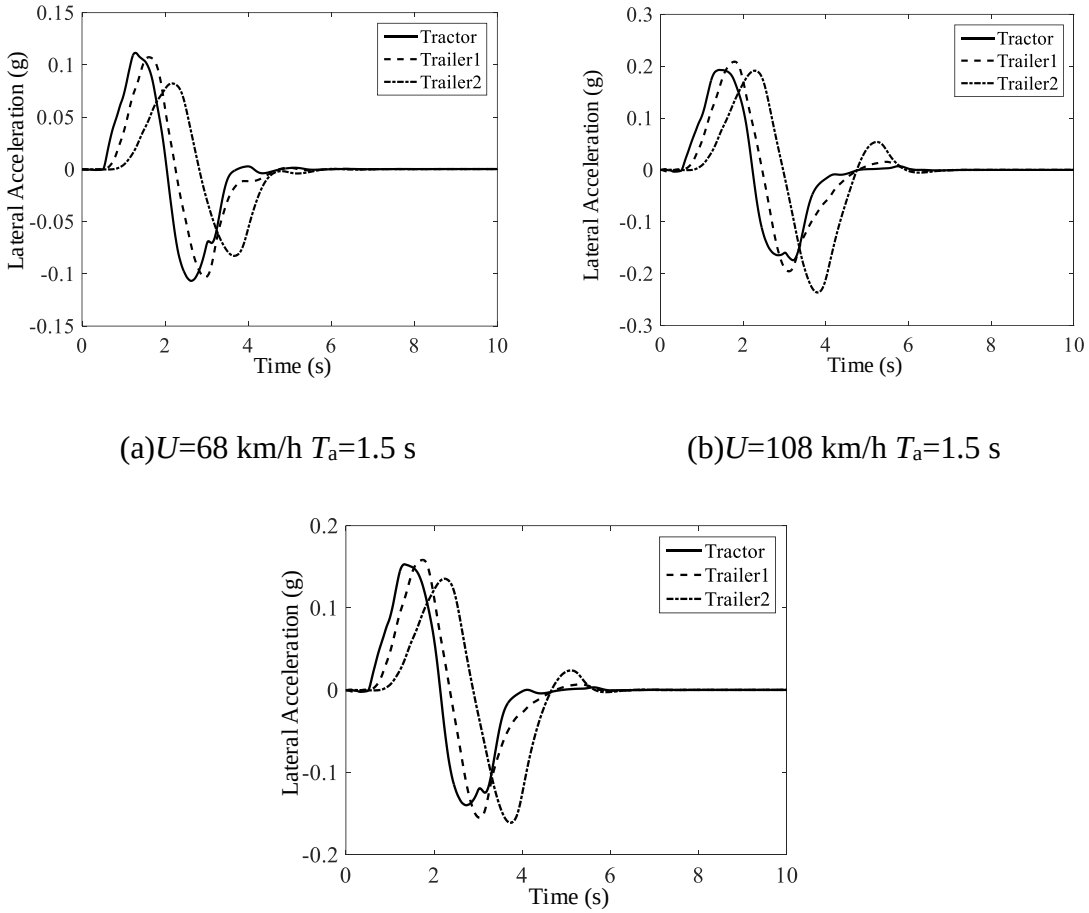

(a)U=68 km/h T_a=1.5 s (b)U=108 km/h T_a=1.5 s

(c)U=88 km/h T_a=1.5 s

Figure 5.10 Performance of A-train with designed ATS under different speeds

Compared with the performance of the A-train without ATS, the lateral accelerations of the both 1st trailer and 2nd trailer decrease dramatically with LQR-LMI ATS controller under the same situation.

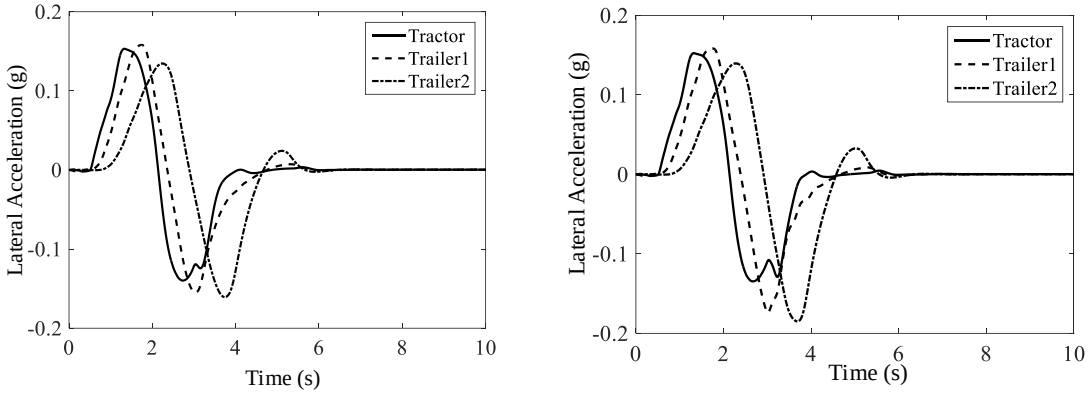

(a)U=88 km/h T_a=0.5 s (b)U=88 km/h T_a=2.5 s

Figure 5.11 Performance of A-train with designed ATS under axle time parameter

As is shown in Fig5.11, the peak lateral acceleration value of the 2nd trailer increases as the time parameter of the active axle rises because the reaction speed of the active axle decreases. The acceleration amplitude of the rearmost trailer reaches 0.187 g when the time parameter of the active axle rises to 2.5 s.

To validate the ATS controller designed by LQR-LMI method with GA optimization. The feedback matrix **K** listed in (5.32) is also simulated with UOIT ATS vehicle experimental platform. The simulation results of the hardware in loop system are shown in Fig 5.12. Compared with A-train without ATS, the lateral accelerations of both trailers with ATS controller decrease dramatically. Under 88 km/h forward speed, the peak lateral

acceleration of the rearmost trailer has already reduced around 40.7% from 0.307g to 0.182g. Even though the hardware in loop simulation results show some differences compared with numerical simulation results, the deviation is still acceptable. The differences may be caused by active axle system and the noise of the hardware system.

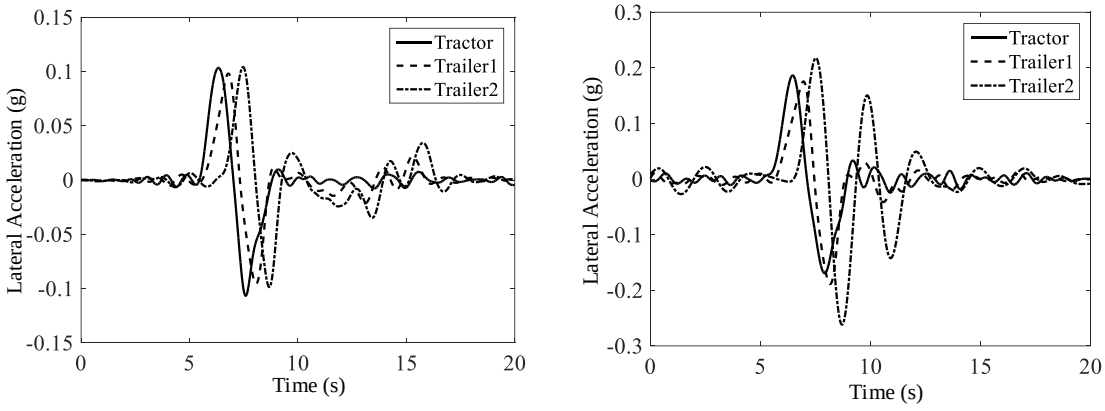

(a)U=68km/h

(b)U=108km/h

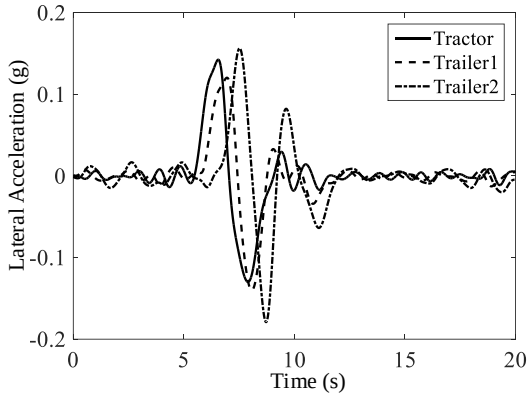

(c)U=88km/h

Figure 5.12 Performance of A-train hardware in loop

To evaluate the performance of designed ATS system, the transient RA curve is obtained via the test maneuver listed in chapter 4 since RA measure is a good indicator for lateral dynamic at high speeds. The numerical simulation RA curves obtained from open-loop without ATS controller and closed-loop with ATS controller are shown in Fig 5.13. Beyond that, the RA curve is also obtained in the hardware simulation platform to validate the numerical simulation.

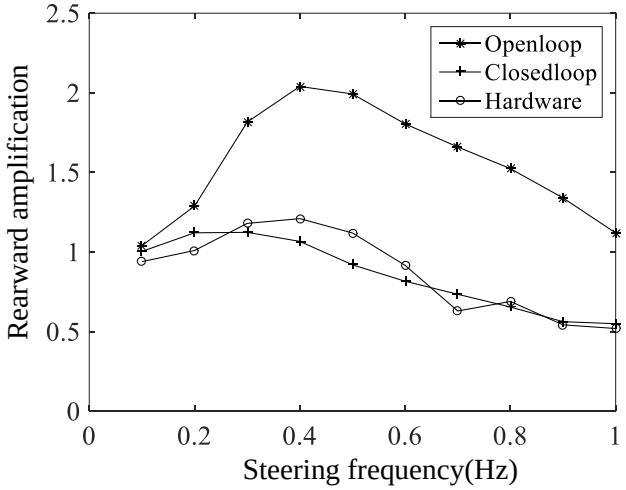

Figure 5.13 RA curve comparison

The RA curves with designed ATS tend to be flatter and lower than that of A-train double without ATS. It is convincing to conclude that the ATS designed from LQR-LMI with GA optimization not only reduces the RA measure dramatically but presents good robust stability. The proposed method is applicable to time-varying uncertain parameters and avoids the frequency sweep needed in H_∞ analysis.

5.4.3 Obstacle Avoidance Ability

To investigate the obstacle avoidance ability of A-train at high speed, the vehicle is tested in such a maneuver that it translates sideways and ends up heading in the original direction of travel. The path chosen for used is designed corresponding to one full cycle of a sine wave lateral acceleration. The mathematic expression of the designed trajectory is shown in (4.2). In this study, the driver model in TruckSim is employed with the preview time 0.25 s [48]. Path with lateral displacement of 1.463 m is laid out and investigated at 88 km/h. The experimental trajectories of the axle 1, 5 and target trajectory are shown in Fig 5.14. The rearmost axle 5 tends to achieve larger off-track distance. And the maximum off-track distance of axle 5 decreases from 34.34 cm without ATS to 10.38 cm with the designed ATS. The maneuverability of the A-train increases a great deal at high speed.

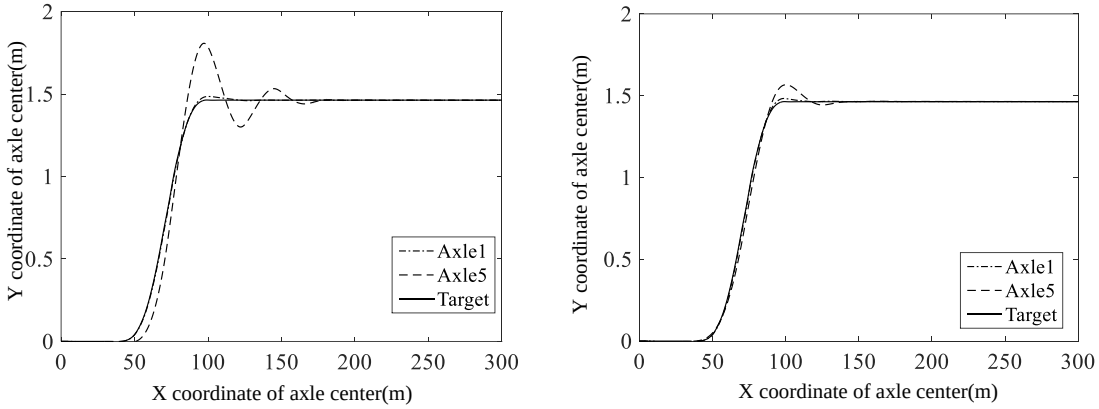

(a)Without ATS (b)With ATS

Figure 5.14 Obstacle avoidance maneuver

To study the influences from the different active steering axles, the same maneuver is repeated under different axle time parameters T_a. The trajectory at the center of the rearmost axle 5 is shown in Fig 5.15. The maximum off-track distance of the axle 5 decreases from 13.2 cm to 10.1 cm when the axle time parameter T_a decreases from 2.5 s to 0.5 s.

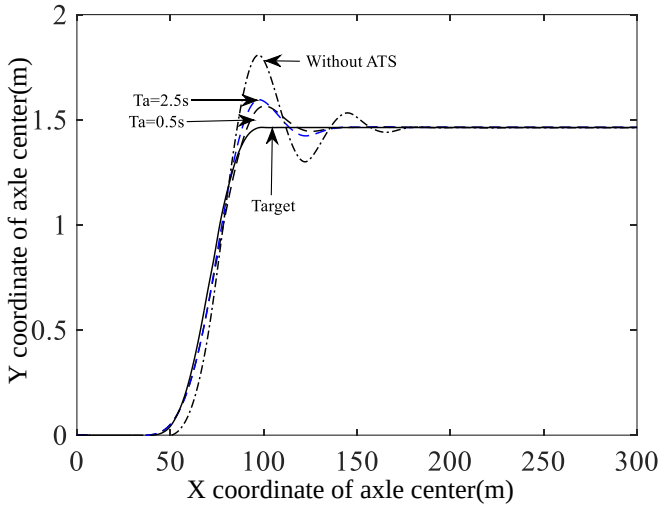

Figure 5.15 Trajectory of axle 5 under different active steering axle

The obstacle avoidance ability of the A-train double is researched under different lateral avoidance displacements in a certain range. The target trajectories for different lateral displacements are designed according to formula (4.2). The maximum off-track distance of the axle 5 versus different lateral displacements is shown in Fig 5.16. It is interesting to point out that the axle 5's off-track distance get its maximum under 0.94 m lateral obstacle maneuver at 88 km/h. With the designed ATS, the maneuverability and trajectory following ability increase a great deal. The maximum off-track distance of axle 5 decreases 65.5% from 34.52 cm to 11.87 cm during 0.94 m lateral obstacle maneuver.

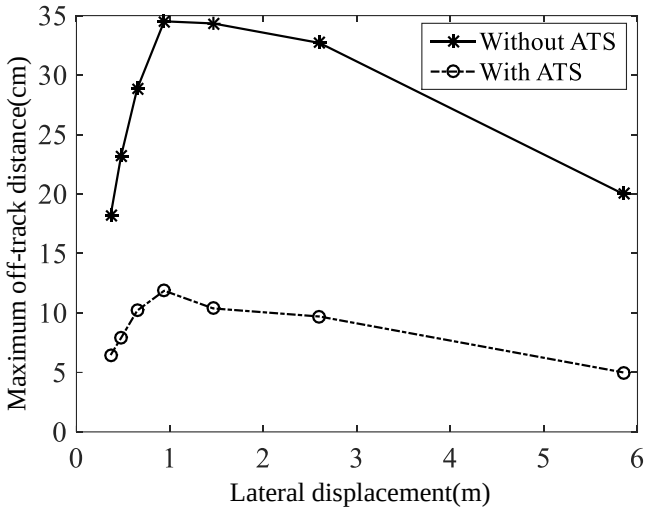

Figure 5.16 Maximum off-track distance versus different lateral displacement

All in all, the designed ATS through robust LQR-LMI method have increased not only the A-train's lateral stability, robust but also improved the trajectory following ability and obstacle avoidance ability at highway speeds. For high speed A-train ATS design, the ATS controller enters into the RA control mode, the RA and lateral acceleration are suppressed. What's more, the maximum off-track distance is also improved as a byproduct since the lateral transient response is suppressed by the designed ATS controller.

Chapter 6

H_∞ Based ATS Controller

6.1 Introduction

Robustness is of vital importance in designing the control-system because real systems are vulnerable to external disturbances, noise and there are always differences between the simplified mathematical models used for designing the controller and the real-world plants. A well-designed controller will not only stabilize a plant but meet the performance level in the presence of certain disturbances as well.

The H_∞ optimal control theory was conducted in early 1980s by Zames and Zames and Francis [49-50]. In the H_∞ control approach, the model of system uncertainty is specified. The algorithm is performed to maximize the robust stability of the closed-loop system to the type of uncertain chosen, the constrain being the internal stability of the feedback system.

In this chapter, the ATS for A-train double at highway speed is designed through H_∞ method, the performance of A-train double with designed ATS is evaluated by RA curves and maximum off-track distance at highway speed.

6.2 H_∞ ATS Controller Design

6.2.1 H_∞ Theory

The H_∞ norm of a system describes the maximum energy gain of the system and is decided by the peak value of the largest singular value of the frequency response matrix over the whole frequency axis. This norm is called H_∞ norm of a system which can be expressed mathematically by matrix norm as follow,

$$\|\mathbf{G}\|_\infty \triangleq \max \sigma_{\max}\left(\mathbf{G}(s)\right) \tag{6.1}$$

To analyze robust stability of the system, the system is rearranged to the M-Δ uncertainty configuration shown in Fig 6.1. The standard uncertainty configuration to present how the uncertainty affects the control system is shown in matrix Δ [51].

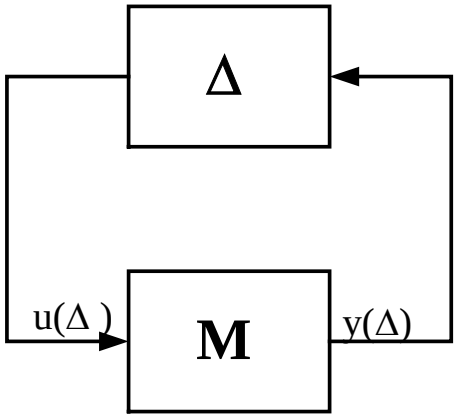

Figure 6.1 Standard M-Δ uncertainty configuration

Many dynamic perturbations that may occur in different parts of a system can, however, be lumped into single perturbation block Δ. The uncertainty representation is referred to as

"unstructured" uncertainty. In the case of linear, time-invariant systems, the block Δ may be represented by an unknown transfer function matrix. The Small-Gain Theorem [52] provides a sufficient condition for robust stability and therefore potentially conservative. The M-Δ in Fig 6.1 is stable for all allowed perturbations if and only if

$$\rho(M\Delta(j\omega)) < 1, \quad \forall \omega, \forall \Delta \tag{6.2}$$

In which ρ is the spectral radius. The standard LTI feedback optimization setup can be described by the block diagram from Fig 6.2. In this diagram, block *P* represents the plant, an LTI model defined by a finite dimensional state space model.

$$\dot{x}(t) = \mathbf{A}x(t) + \mathbf{B_1}\omega(t) + \mathbf{B_2}u(t) \tag{6.3}$$

$$e(t) = \mathbf{C_1}x(t) + \mathbf{D_{11}}\omega(t) + \mathbf{D_{12}}u(t) \tag{6.4}$$

$$y(t) = \mathbf{C_2}x(t) + \mathbf{D_{21}}\omega(t) + \mathbf{D_{22}}u(t) \tag{6.5}$$

Where the coefficient matrices $\mathbf{A}$, $\mathbf{B_i}$, $\mathbf{C_i}$, $\mathbf{D_{ik}}$ are known. In turn, the block *K* represents the controller, an LTI model defined by a finite dimensional state space model.

$$\dot{x}_f(t) = \mathbf{A_f}x_f(t) + \mathbf{B_f}y_f(t) \tag{6.6}$$

$$u_f(t) = \mathbf{C_f}x_f(t) + \mathbf{D_f}y_f(t) \tag{6.7}$$

Where the coefficients $\mathbf{A_f}$, $\mathbf{B_f}$, $\mathbf{C_f}$, $\mathbf{D_f}$ are to be designed with the feedback matrix *K*.

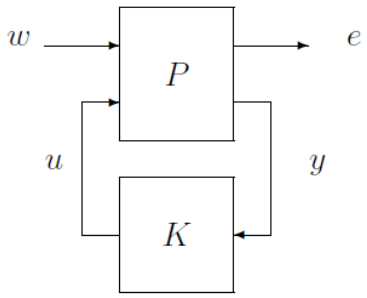

Figure 6.2 P-K configuration

Then the matrix **P** can be expressed as

$$\mathbf{P} = \begin{bmatrix} \mathbf{P_{11}} & \mathbf{P_{12}} \\ \mathbf{P_{13}} & \mathbf{P_{14}} \end{bmatrix} = \begin{bmatrix} \mathbf{A} & \mathbf{B_1} & \mathbf{B_2} \\ \mathbf{C_1} & \mathbf{D_{11}} & \mathbf{D_{12}} \\ \mathbf{C_2} & \mathbf{D_{21}} & \mathbf{D_{22}} \end{bmatrix} \tag{6.8}$$

Consider a continuous linear time-invariant plant **P** mapping exogenous disturbance input *w* and control inputs *u* to outputs *e* and the measured output *y*. In Laplace domain, that is

$$\begin{bmatrix} E(s) \\ Y(s) \end{bmatrix} = \begin{bmatrix} P_{11}(s) & P_{12}(s) \\ P_{21}(s) & P_{22}(s) \end{bmatrix} \begin{bmatrix} W(s) \\ U(s) \end{bmatrix} \tag{6.9}$$

Given output feedback as follow:

$$U(s) = \mathbf{K}(s)Y(s) \tag{6.10}$$

With the assumption of zero initial condition of the state variables and using Laplace transform, a closed-loop transfer function *F*(*P*,*K*) from disturbance *w* to controlled output error *e* is

$$F(P,K) = P_{11} + P_{12}K(I - P_{22}K)^{-1}P_{21} \tag{6.11}$$

The suboptimal H∞ control problem of finding a controller **K**(s) is identical to the problem of optimization problem:

1. The closed-loop system is internally stable
2. Minimize the maximum gain from disturbance *w* to error *e* $\|F(P,K)\|_\infty$

The optimization of the H_∞ norm of the function can be solved by Bounded Real Lemma for continuous system as follow.

Lemma 6.1 Consider a continuous-time transfer function *G*(s) of closed loop system, $G(s) = \mathbf{D_{cl}} + \mathbf{C_{cl}}(\mathbf{sI} - \mathbf{A_{cl}})^{-1}\mathbf{B_{cl}}$. The following statements are equivalent [53-56]:

1. $\left\|\mathbf{D_{cl}} + \mathbf{C_{cl}}(\mathbf{sI} - \mathbf{A_{cl}})^{-1}\mathbf{B_{cl}}\right\|_\infty < \gamma$ and $\mathbf{A_{cl}}$ is stable in the continuous-time sense (real part of A eigenvalues are negative);
2. There exist a symmetric positive definite solution **X** to LMI:

$$\begin{pmatrix} \mathbf{A_{cl}^T X + X A_{cl}} & \mathbf{X B_{cl}} & \mathbf{C_{cl}^T} \\ \mathbf{B_{cl}^T X} & -\gamma\mathbf{I} & \mathbf{D_{cl}^T} \\ \mathbf{C_{cl}} & \mathbf{D_{cl}} & -\gamma\mathbf{I} \end{pmatrix} < 0 \qquad (6.12)$$

3. From the Schur decomposition, the second statement can be simplified as: There exists a symmetric positive definite solution **X** to LMI:

$$\begin{aligned} &\sigma_{\max}(\mathbf{D_{cl}}) < \gamma \\ &\mathbf{A_{cl}^T X + X A_{cl}} + \gamma^{-1}\mathbf{C_{cl}^T C_{cl}} + \gamma(\mathbf{X B_{cl}} + \gamma^{-1}\mathbf{C_{cl}^T D_{cl}})(\gamma^2\mathbf{I} - \mathbf{D_{cl}^T D_{cl}})^{-1}(\mathbf{B_{cl}^T X} + \gamma^{-1}\mathbf{D_{cl}^T C_{cl}}) < 0 \end{aligned} \qquad (6.13)$$

From lemma 6.1, it is interesting to figure out that the continuous-H_∞ control problems are solved via Riccati inequalities. Thanks to such connections, the LMI-based characterization of H_∞ controllers opens new perspectives for the refinement of H_∞ design.

6.2.2 ATS Controller of A-train

The exogenous disturbance δ is weighted by the frequency function $\mathbf{W_{d1}}$, the output vector $\begin{bmatrix} a_{y3} & a_{y4} \end{bmatrix}^T$ by $\mathbf{W_p}$, the control input u by $\mathbf{W_{p1}}$, and the measurement noise **d** by $\mathbf{W_d}$. A H_∞ controller $\mathbf{K}$ intends to minimize the H_∞ norm from the disturbance inputs δ and **d** to the performance signals $\mathbf{e_p}$ and $\mathbf{e_{p1}}$.

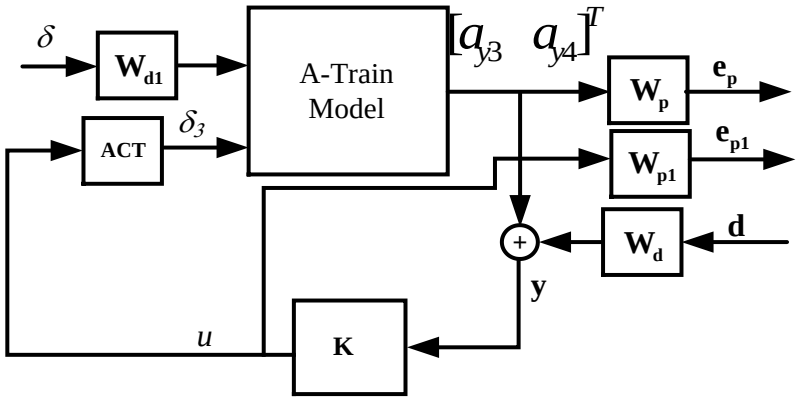

Figure 6.3 Control structure with frequency weighting functions

$\mathbf{W_{d1}}$ is the weight function of the driver's steering wheel. It is chosen to be a constant. $\mathbf{W_d}$ models broadband sensor noise of intensity. $\mathbf{W_p}$ is shown as follow,

$$\mathbf{W_p} = diag\left(\begin{bmatrix} \dfrac{s/M_1 + w_{b1}}{s + w_{b1}A_1} & \dfrac{s/M_2 + w_{b2}}{s + w_{b2}A_2} \end{bmatrix}\right) \tag{6.14}$$

To improve high frequency rejection of the actuator, $\mathbf{W_{p1}}$ is chosen to be a high-pass filter that limits the control input at high frequencies and closed-loop bandwidth. Considering the reaction of the actuator, the $\mathbf{W_{p1}}$ is chosen as follow,

$$\mathbf{W}_{\mathbf{p1}} = \frac{s^2}{s^2 + \sqrt{2}s + 1} \tag{6.15}$$

6.3 Simulation Result of H∞ ATS

The ATS controller is designed through H∞ method in Matlab toolbox. The ATS is designed under the condition that the forward speed $U \in [68 \quad 108]$ km/h and active axle time parameter $T_a \in [0.5 \quad 2.5]$ s. The designed H∞ controller satisfies the robust stability requirements under the given parameter disturbances. Furthermore, the lateral acceleration of the first and second trailers are chosen to be the performance index. Then, the H∞ controller will minimize the H∞ norm from the driver's steering input and disturbances to the lateral acceleration of the trailers. In order to validate the designed controller, the sine wave input steering test maneuver is applied to A-train double with the ATS controller in TruckSim.

The lateral accelerations and the yaw rates of both the tractor and trailers are shown in Fig 6.4 under the designed ATS controller when the forward speed is chosen to be 88 km/h and active axle parameter to be 1.5 s. The amplitude of the acceleration of the 2nd trailer is

reduced dramatically from 0.307 g to 0.197 g with the ATS controller. Compared with the yaw rate without controller, the peak yaw rate of the 2nd trailer under the designed ATS controller also decreases from 7.38 deg/s to 4.7 deg/s. The simulation results reveal that the ATS controller designed through H_∞ method works well in the conditions that forward speed 88km/h and active axle time parameter 1.5s.

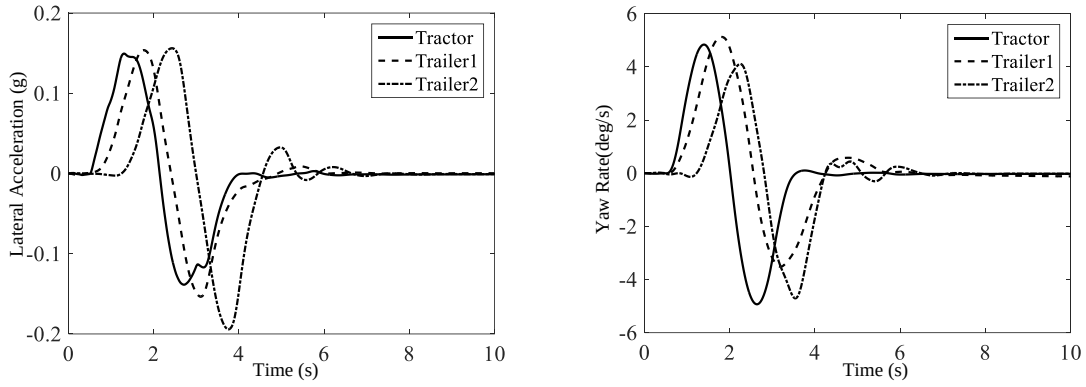

(a)Lateral acceleration (b)Raw rate

Figure 6.4 Simulation results of ATS controller under U=88km/h T_a=1.5s

In order to validate the robust stability of the designed ATS controller, the sine wave steering input is applied to the front axle under different forward speed ranging from 68km/h to 108km/h and the active axle time parameter ranging from 0.5s to 2.5s. The lateral accelerations of the tractor and the trailers are shown in Fig 6.5.

The accelerations of the tractor and trailers incline to increase when the forward speed rises from 68 km/h to 108 km/h. However, compared with the A-train without ATS controller,

the acceleration amplitudes of the tractor and trailers are both reduced dramatically. With the increasing of the active axle time parameter from 0.5 s to 2.5 s, the lateral acceleration of the 2nd trailer starts to increase. This is easy to understand because the active axle's reaction time increases as the active axle time parameter increases.

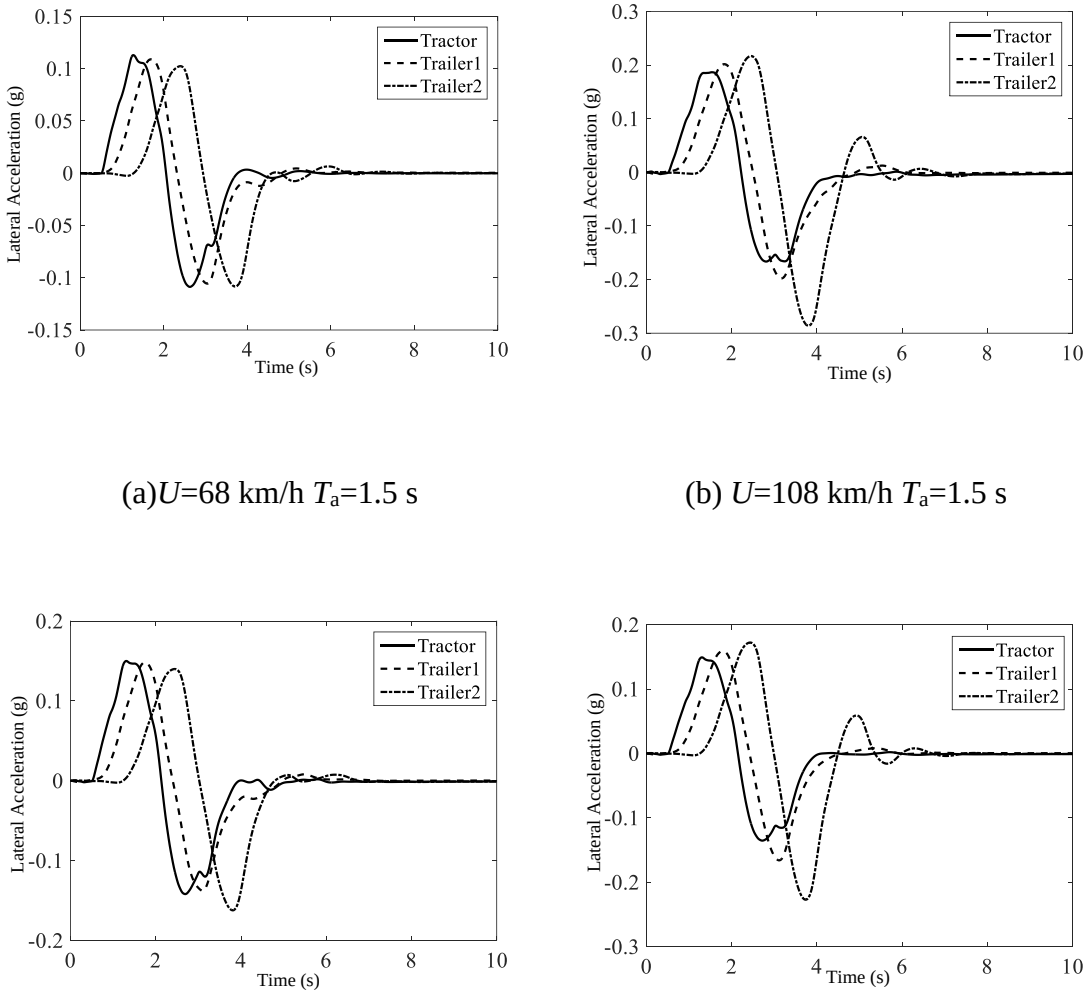

(a)U=68 km/h T_a=1.5 s (b) U=108 km/h T_a=1.5 s

(c)U=88 km/h T_a=0.5 s (d)U=88 km/h T_a=2.5 s

Figure 6.5 Robust stability performance of ATS

From the Fig 6.5, the designed H_∞ controller shows good robust stability performance and has the tendency to decrease the lateral acceleration of the trailers. In order to evaluate the ATS, the transient RA curves of the A-train double under the designed controller is obtained under the ISO standards illustrated in chapter 4.

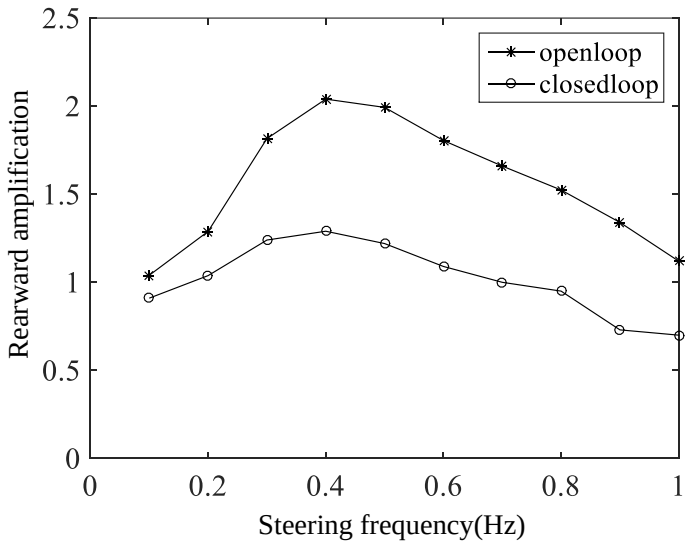

Figure 6.6 RA curve of ATS designed by H_∞

From the Fig 6.6, the ATS reduces RA measure 36.8% from 2.04 to 1.29 under the 0.4 Hz steering frequency. It is adequate to conclude that the designed ATS is able to reduce the RA measures dramatically and thus increasing the lateral performance of the A-train based on the ISO standard. With lower RA measures, the A-train double acquires more obstacle avoidance ability and less opportunity to rollover. All in all, the ATS is a promising equipment to increase the lateral dynamic performance of the A-train double in high speed.

The obstacle avoidance ability is also evaluated through the same method illustrated in details in chapter 5.4.3. The forward speed is chosen 88 km/h. During the 1.463 m lateral displacement maneuver, the axle 1, 5 and target trajectories are shown in Fig 6.7. Maximum off-track distance reduces 44.5% from 34.34cm without ATS to 19cm with designed ATS.

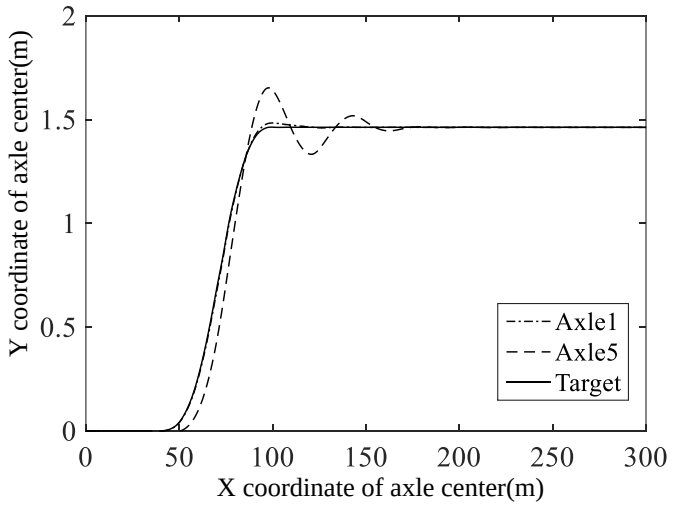

Figure 6.7 Trajectory of different axle

To investigate the effect brought about by active steering axles, the same maneuver is repeated under different axle's time parameters. The simulation result is illustrated in Fig 6.8 in details. With the increasing of the active axle's time parameter T_a, the maximum off-track distance of axle 5 tend to rises.

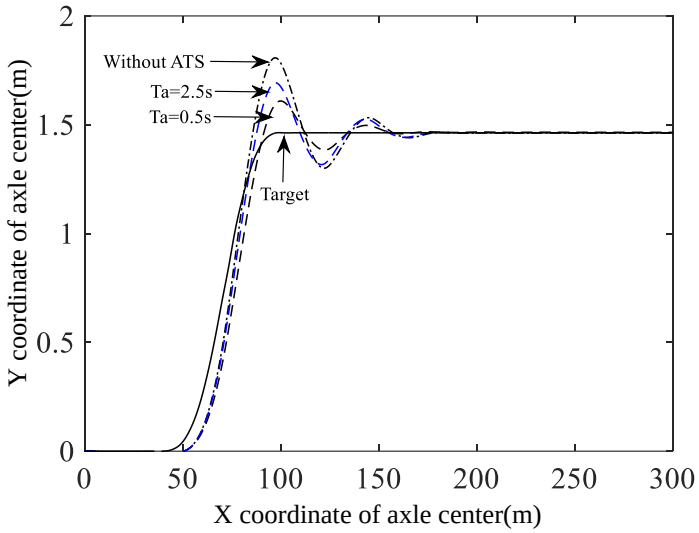

Figure 6.8 Trajectory of axle 5 under different active steering axle

In conclusion, the designed ATS works well in high speed to suppress the lateral accelerations and RA of A-train at highway speed. The trajectory following ability in high speed is also improved due to the elimination of the transient response of the lateral acceleration by designed ATS.

Chapter 7

Conclusions

As discussed in Chapter 1, although the application of A-train double can bring about economic and environmental benefits, however, it has been reported that A-train double shows poor lateral dynamic because of their complex structure. RA is introduced by ISO to quantify and indicates the lateral dynamic of LCVs. The LCVs with smaller RA will show more obstacle avoidance ability and less opportunity to rollover. In chapter 4, three RA test maneuvers are studied based on A-train double. The inconsistency of the listed methods is discussed in detail. In chapter 5 and 6, an ATS system is devised and validated by numerical simulation and hardware simulation. The conclusion are drawn as follow:

1. The RA measure difference between time domain methods and frequency domain test method mainly comes from the transient response of the LCVs. For closed-loop trajectory following method, different driving habits impose non-neglected influence on steering wheel input waveform and eventually instigate different level transient response of the LCVs lateral motion.
2. ATS designed from both LQR-LMI with GA optimization and H_∞ method not only reduce the RA measure dramatically but present good robust stability.

3. The proposed LQR-LMI method with GA optimization is applicable to time-varying uncertain parameters and avoids the frequency sweep needed in H_∞ analysis which will simply the design process.

References

[1] Ontario's long combination vehicle program - Ontario trucking association(2016) Available at: http://ontruck.org/ota-classroom-training/ontarios-long-combination-vehicle-program/.

[2] The province of New Brunswick, Canada, its natural resources and development (1930b) Journal of the Franklin Institute, 210(1), p. 126. doi: 10.1016/s0016-0032(30)90842-3.

[3] Uffelmann, F. "Automotive stability and handling dynamics in cornering and braking maneuvers." Vehicle System Dynamics 12.4-5 (1983): 203-223.

[4] Ervin, R. D. "The dependence of truck roll stability on size and weight variables." International Journal of Vehicle Design7.5-6 (1986): 192-208.

[5] Winkler, Christopher B., and R. D. Ervin. Rollover of heavy commercial vehicles. No. UMTRI-99-19,. University of Michigan, Transportation Research Institute, 1999.

[6] Billing, John R., and J. D. Patten. "An assessment of tank truck roll stability." International Symposium on Heavy Vehicle Weights and Dimensions. 2006.

[7] John Aurell and Jacco Koppenaal. "Simplified procedure for determining lateral stability of heavy vehicle combinations", Road Transport Technology-4,

Proceedings of the fourth international symposium on heavy vehicle weighs and dimensions, Ann Arbor, USA, 1995.

[8] Winkler, C. B., et al. "Heavy vehicle size and weight-test procedures for minimum safety performance standards." (1992).

[9] Fancher PS, Winkler CB. A methodology for measuring rearward amplification. Proceedings of the 3rd International Symposium on Heavy Vehicle Weights and Dimensions. Queens College, Cambridge, United Kingdom; 1992.

[10] J. Woodrooffe and P. Milliken, "Safety Analysis of A Double & Triple B-Train Carrying Loaded Containers", Report for Saskatchewan Highways and Transportation, Woodrooffe & Associates Incorporated; 2007.

[11] J. Preston-Thomas and M. El-Gindy. "Path compliance in lane-change tests designed to evaluate rearward amplification", Road Transport Technology-4, Proceedings of the fourth international symposium on heavy vehicle weighs and dimensions, Ann Arbor, USA, 1995.

[12] M. Islam, "Parallel Design Optimization of Multi-Trailer Articulated Heavy Vehicle with Active Safety Systems" PhD Thesis, University of Ontario Institute of Technology, Oshawa, Ontario, Canada, 2013.

[13] Qiushi. Wang, "Design and Validation of Active Trailer Steering Systems for Articulated Heavy Vehicles Using Driver-Hardware-in-the-Loop Real-Time

Simulation" Master Thesis, University of Ontario Institute of Technology, Oshawa, Ontario, Canada, 2015.

[14] Winkler, C. B., et al. "Heavy vehicle size and weight-test procedures for minimum safety performance standards." (1992).

[15] X. Ding, S. Mikaric, and Y. He, "Design of An Active Trailer Steering System for Multi-Trailer Articulated Heavy Vehicles Using Real-Time Simulations", Journal of Automobile Engineering, 2013, Vol, 227(5), pp. 643-655.

[16] Wang, Rongrong, Hui Zhang, and Junmin Wang. "Linear parameter-varying controller design for four-wheel independently actuated electric ground vehicles with active steering systems." IEEE Transactions on Control Systems Technology 22(4) (2014): 1281-1296.

[17] Cheng, Caizhen, and David Cebon. "Improving roll stability of articulated heavy vehicles using active semi-trailer steering." Vehicle System Dynamics 46.S1 (2008): 373-388.

[18] Hiraoka, Toshihiro, Osamu Nishihara, and Hiromitsu Kumamoto. "Model-following sliding mode control for active four-wheel steering vehicle." Review of Automotive Engineering 25.3 (2004): 305.

[19] ISO-14791, 2000, International Organization for Standardization. Road vehicles – Heavy commercial vehicle combinations and articulated buses – Lateral stability

test methods. ISO-14791:2000(E), Geneva: International Organization for Standardization; 2000

[20] Wang, Qiushi, and He, Yuping, 2015, A Study on Single Lane Change Maneuvers for Determining Rearward Amplification of Multitrailer Articulated Heavy Vehicles with Active Trailer Steering Systems, To Appear in Vehicle System Dynamics

[21] Corporation, M.S. (2005) TruckSim options. Available at: https://www.carsim.com/products/trucksim/packages.php (Accessed: 19 July 2016).

[22] Zhu, Shenjin and He, Yuping, 2015, Articulated Heavy Vehicle Lateral Dynamic Analysis Using an Automated Frequency Response Measuring Technique, International Journal of Vehicle Performance

[23] Hespanha, J.P. (2005) Lecture notes on LQR/LQG controller design. Available at: http://www.uz.zgora.pl/~wpaszke/materialy/kss/lqrnotes.pdf.

[24] Lecture notes on control of surface and underwater vehicle Available at: http://ocw.mit.edu/courses/mechanical-engineering/2-154-maneuvering-and-control-of-surface-and-underwater-vehicles-13-49-fall-2004/lecture-notes/lec19.pdf .

[25] Cheng, Caizhen, and David Cebon. "Improving roll stability of articulated heavy vehicles using active semi-trailer steering." Vehicle System Dynamics46.S1 (2008): 373-388.

[26] He, Y., Islam, M., and Webster, T., "An Integrated Design Method for Articulated Heavy Vehicles with Active Trailer Steering Systems," SAE Int. J. Passeng. Cars – Mech. Syst.3(1):158-174, 2010, doi:10.4271/2010-01-0092.

[27] Chang, Sheng, et al. "H∞ Loop Shaping Robust Control For Tractor-semitrailer." MATEC Web of Conferences. Vol. 34. EDP Sciences, 2015.

[28] Jin, Zhilin, et al. "Stability and optimised H∞ control of tripped and untripped vehicle rollover." Vehicle System Dynamics (2016): 1-23.

[29] BAGLEY, J. D. The Behavior of Adaptive Systems Which Employ Genetic and Correlative Algorithms. PhD thesis, University of Michigan, Ann Arbor, 1967.

[30] HOLLAND, J. H. Adaptation in Natural and Artificial Systems, first MIT Press ed. The MIT Press, Cambridge, MA, 1992. First edition: University of Michigan Press, 1975.

[31] HOLLAND, J. H., HOLYOAK, K. J., NISBETT, R. E., AND THAGARD, P. R. Induction: Processes of Inference, Learning, and Discovery. Computational Models of Cognition and Perception. The MIT Press, Cambridge, MA, 1986.

[32] Sanz, Ricardo. "Intelligence, control and the artificial mind." (2010).

[33] Demir O, Keskin I, Cetin S. Modeling and control of a nonlinear half-vehicle suspension system: a hybrid fuzzy logic approach. Nonlinear Dynamics. 2012 Feb 1;67(3):2139-51.

[34] Schouten NJ, Salman MA, Kheir NA. Fuzzy logic control for parallel hybrid vehicles. IEEE transactions on control systems technology. 2002 May;10(3):460-8.

[35] [35]Mon YJ, Lin CM. Supervisory recurrent fuzzy neural network control for vehicle collision avoidance system design. Neural Computing and Applications. 2012 Nov 1;21(8):2163-9.

[36] Corporation, M.S. (2005) TruckSim overview. Available at: https://www.carsim.com/products/trucksim/.

[37] Corporation2016Pololu (2001) Pololu robotics and electronics. Available at: https://www.pololu.com/

[38] Nise, N.S. (2011) Control systems engineering. 6th edn. United Kingdom: John Wiley & Sons.

[39] Da-Wei, G., Petkov, P., Konstantinov, M.M., Gu, D.-W. and Petkov, H.P. (2005) Robust control design with MATLAB. United Kingdom: Springer-Verlag New York.

[40] Hespanha, Joao P. Linear systems theory. Princeton university press, 2009.

[41] Rajamani, R. (2005) Vehicle dynamics and control. New York: Springer-Verlag New York.

[42] Khalil, Hassan K., and J. W. Grizzle. Nonlinear systems. Vol. 3. New Jersey: Prentice hall, 1996.

[43] E. Feron, V. Balakrishnan, S. Boyd, and L. EI Ghaoui, “Numerical methods for H2 related problem,” in Proc. ACC, 1992, pp.2921-2922

[44] Gahinet P, Apkarian P, Chilali M. Affine parameter-dependent Lyapunov functions and real parametric uncertainty. IEEE Transactions on Automatic control. 1996 Mar;41(3):436-42.

[45] Rowell, D. (2002) Time-domain solution of LTI state equations. Available at: http://web.mit.edu/2.14/www/Handouts/StateSpaceResponse.pdf.

[46] Olalla, Carlos, et al. "Robust LQR control for PWM converters: an LMI approach." IEEE Transactions on industrial electronics 56.7 (2009): 2548-2558.

[47] Feron, E., et al. "Numerical methods for H2 related problems." Proc. American Control Conf. Vol. 4. 1992.

[48] McLean JR, Hoffmann ER. The effects of restricted preview on driver steering control and performance. Human Factors: The Journal of the Human Factors and Ergonomics Society. 1973 Aug 1;15(4):421-30.

[49] Zames, G.: Feedback and optimal sensitivity: model reference transformations, multiplicative seminorms and approximate inverses. IEEE Trans. Autom. Control AC-26, 301–320 (1981)

[50] Zames, G., Francis, B.A.: Feedback, minimax sensitivity, and optimal robustness. IEEE Trans. Autom. Control AC-28, 585–600 (1983)

[51] Skogestad, S., & Postlethwaite, I. (2007).Multivariable feedback control: analysis and design (Vol. 2). New York: Wiley.

[52] Gu, Da-Wei, Petko Petkov, and Mihail M. Konstantinov. Robust control design with MATLAB®. Springer Science & Business Media, 2005.

[53] Glover, K., and J.C. Doyle, "State-space formulae for all stabilizing controllers that satisfy an H∞ norm bound and relations to risk sensitivity," Systems & Control Letters, vol. 11, no. 8, pp. 167–172, 1988.

[54] Doyle, J.C., K. Glover, P. Khargonekar, and B. Francis, "State-space solutions to standard H2 and H∞ control problems," IEEE Transactions on Automatic Control, vol. 34, no. 8, pp. 831–847, August 1989

[55] Safonov, M.G., D.J.N. Limebeer, and R.Y. Chiang, "Simplifying the H∞ Theory via Loop Shifting, Matrix Pencil and Descriptor Concepts",Int. J. Contr., vol. 50, no. 6, pp. 2467-2488, 1989.

[56] Iwasaki, T., and R.E. Skelton, "All controllers for the general H∞-control problem: LMI existence conditions and state space formulas," Automatica, vol. 30, no. 8, pp. 1307–1317, 1994.

Appendix

Appendix 1: Nomenclature and Parameter Values of A-Train

Symbol	Description	Value
m_1	Total mass of the tractor	5760kg
m_{t1}	Total mass of the first semitrailer	12665kg
m_d	Total mass of the dolly	1140kg
m_{t2}	Total mass of the second trailer	12665kg
U	Forward speed of the vehicle	m/s
V_1	Lateral speed of the tractor	m/s
V_2	Lateral speed of the first semitrailer	m/s
V_3	Lateral speed of the dolly	m/s
V_4	Lateral speed of the second trailer	m/s
r_1	Yaw rate of the tractor	rad/s
r_2	Yaw rate of the first semitrailer	rad/s
r_3	Yaw rate of the dolly	rad/s
r_4	Yaw rate of the second semitrailer	rad/s
I_1	Yaw moment of inertia of the tractor	39,214kg m^2
I_{t1}	Yaw moment of inertia of the first semitrailer	55,815kg m^2

Symbol	Description	Value
I_d	Yaw moment of inertia of the dolly	371kg m^2
I_{t2}	Yaw moment of inertia of the second trailer	55,815kg m^2
Ψ_1	Yaw angle of the tractor	rad
Ψ_2	Yaw angle of the first semitrailer	rad
Ψ_3	Yaw angle of the dolly	rad
Ψ_4	Yaw angle of the second trailer	rad
$f_1(\alpha_1)$	Lateral force on the front axle of the tractor	N
$f_2(\alpha_2)$	Lateral force on the rear axle of the tractor	N
$f_3(\alpha_3)$	Lateral force on the axle of the first semitrailer	N
$f_4(\alpha_4)$	Lateral force on the axle of the dolly	N
$f_5(\alpha_5)$	Lateral force on the axle of the second trailer	N
Y_1	Lateral reaction force at the hitch point connecting the tractor and the first semitrailer	N
Y_2	Lateral reaction force at the hitch point connecting the first semitrailer and the dolly	N
Y_3	Lateral reaction force at the hitch point connecting the dolly and the second trailer	N
α_1	Side-slip angle of the front axle of the tractor	rad

Symbol	Description	Value
α_2	Side-slip angle of the rear axle of the tractor	rad
α_3	Side-slip angle of the first trailer's axle	rad
α_4	Side-slip angle of the dolly's axle	rad
α_5	Side-slip angle of the second trailer's axle	rad
a	Longitudinal distance between front axle and the CG of the tractor	1.11m
b	Longitudinal distance between the CG and the first rear axle of the tractor	2.39m
e	Longitudinal distance between the CG of the first semitrailer and the first hitch point	3.5m
h	Longitudinal distance between the CG of the first semitrailer and the first semitrailer's axle	3.2m
j	Longitudinal distance between the CG of the first semitrailer and the second hitch point	4.315m
e'	Longitudinal distance between the CG of the dolly and the second hitch point	1.8m
h'	Longitudinal distance between the CG of the dolly and the dolly's axle	0.3m

Symbol	Description	Value
j'	Longitudinal distance between the CG of the dolly and the third hitch point	0.06m
k	Longitudinal distance between the CG of the second trailer and the third hitch point	3.5m
l	Longitudinal distance between the CG of the second trailer and the second trailer's axle	3.2m
δ	Steer angle of the front axle wheel of the tractor	rad
C_f	Cornering stiffness of the front axle of the tractor	-382,640 N/rad
C_r	Cornering stiffness of the rear axle of the tractor	-540,960 N/rad
C_{t1}	Cornering stiffness of the axle of the first semitrailer	-547,210 N/rad
C_d	Cornering stiffness of the axle of the dolly	-464,990 N/rad
C_{t2}	Cornering stiffness of the axle of the second trailer	-503,570 N/rad

Appendix 2: System Matrices of A-Train

In Equation (3.20), matrices $\mathbf{A} = -\mathbf{M}^{-1}\mathbf{K}$ and $\mathbf{B} = -\mathbf{M}^{-1}\mathbf{N}$. The non-zero elements of the matrices are

$M(1,1) = dm_1$

$M(1,2) = I_1$

$M(2,7) = -km_{t2}$

$M(2,8) = I_{t2}$

$M(3,1) = m_1$

$M(3,3) = m_{t1}$

$M(3,5) = m_d$

$M(3,7) = m_{t2}$

$M(4,1) = (e + j)m_1$

$M(4,3) = jm_{t1}$

$M(4,4) = I_{t1}$

$M(5,5) = -e'm_d$

$M(5,6) = I_d$

$M(5,7) = -(e' + j')m_{t2}$

$M(6,1) = -1$

$M(6,2) = d$

$$M(6,3)=1$$

$$M(6,4)=e$$

$$M(7,3)=-1$$

$$M(7,4)=j$$

$$M(7,5)=1$$

$$M(7,6)=e'$$

$$M(8,5)=-1$$

$$M(8,6)=j'$$

$$M(8,7)=1$$

$$M(8,8)=k$$

$$K(1,1)=\frac{C_f(a+d)+C_r(d-b)}{U}$$

$$K(1,2)=\frac{C_f a(a+d)-C_r b(d-b)}{U}-dm_1U$$

$$K(2,7)=\frac{-(l+k)C_{t2}}{U}$$

$$K(2,8)=\frac{lC_{t2}(l+k)}{U}+km_{t2}U$$

$$K(3,1)=\frac{C_f+C_r}{U}$$

$$K(3,2)=\frac{C_f a-C_r b}{U}-m_1U$$

$$K(3,3)=\frac{C_{t1}}{U}$$

$$K(3,4)=\frac{-C_{t1}h}{U}-m_{t1}U$$

$$K(3,5)=\frac{C_d}{U}$$

$$K(3,6) = \frac{-C_d h'}{U} - m_d U$$

$$K(3,7) = \frac{C_{t2}}{U}$$

$$K(3,8) = \frac{-lC_{t2}}{U} - m_{t2} U$$

$$K(4,1) = \frac{(e+j)(C_f + C_r)}{U}$$

$$K(4,2) = \frac{(e+j)(aC_f - bC_r)}{U} - (e+j)m_1 U$$

$$K(4,3) = \frac{(j-h)C_{t1}}{U}$$

$$K(4,4) = \frac{-hC_{t1}(j-h)}{U} - jm_{t1} U$$

$$K(5,5) = \frac{-(e'+h')C_d}{U}$$

$$K(5,6) = \frac{(e'+h')h'C_d}{U} + e'm_d U$$

$$K(5,7) = \frac{-(e'+j')C_{t2}}{U}$$

$$K(5,8) = \frac{(e'+j')lC_{t2}}{U} + (e'+j')m_{t2} U$$

$$K(6,2) = U$$

$$K(6,4) = -U$$

$$K(7,4) = U$$

$$K(7,6) = -U$$

$$K(8,6) = U$$

$$K(8,8) = -U$$

$$N = [-(a+d)C_f \quad 0 \quad -C_f \quad -(e+j)C_f \quad 0 \quad 0 \quad 0 \quad 0]^T$$